https://ntrs.nasa.gov/search.jsp?R=19770024152 2020-03-22T07:29:53+00:00Z

General Disclaimer

One or more of the Following Statements may affect this Document

- This document has been reproduced from the best copy furnished by the organizational source. It is being released in the interest of making available as much information as possible.

- This document may contain data, which exceeds the sheet parameters. It was furnished in this condition by the organizational source and is the best copy available.

- This document may contain tone-on-tone or color graphs, charts and/or pictures, which have been reproduced in black and white.

- This document is paginated as submitted by the original source.

- Portions of this document are not fully legible due to the historical nature of some of the material. However, it is the best reproduction available from the original submission.

Produced by the NASA Center for Aerospace Information (CASI)

(NASA-CR-135270) OPERATING CHARACTERISTICS OF AN INLET MODEL TESTED WITH A 0.5m POWERED FAN AT HIGH ANGIES OF ATTACK (Boeing Co., Seattle, Wash.) 60 p HC A04/MF A01 CSCL 01A

N77-31096

Unclas
G3/02 47714

NASA CR-135270

CONTRACTOR REPORT

NAS3-20597

SEPTEMBER 1977

OPERATING CHARACTERISTICS OF AN INLET MODEL TESTED WITH A 0.5M POWERED FAN AT HIGH ANGLES OF ATTACK

J.L. Koncsek
Boeing Military Airplane Development
Seattle, WA 98124

R.J. Shaw
Lewis Research Center
Cleveland, Ohio 44135

1. Report No.	2. Government Accession No.	3. Recipient's Catalog No.
NASA CR-135270		

4. Title and Subtitle	5. Report Date
Operating Characteristics of an Inlet Model Tested with a 0.5m Powered Fan at High Angles of Attack	September 1977
	6. Performing Organization Code
7. Author(s)	8. Performing Organization Report No.
J. L. Koncsek and R. J. Shaw	D180-20798-1
	10. Work Unit No.
9. Performing Organization Name and Address	11. Contract or Grant No.
Boeing Military Airplane Development Seattle, Washington 98124	NAS3-20597
	13. Type of Report and Period Covered
12. Sponsoring Agency Name and Address	Contractor Report
National Aeronautics and Space Administration Washington, D. C. 20546	14. Sponsoring Agency Code

15. Supplementary Notes

16. Abstract

An inlet model designed for high angle-of-attack capability, coupled to a .508 m tip diameter turbofan simulator, was tested in the NASA-Lewis Research Center's 9-by 15-ft Low Speed Wind Tunnel. The test variables were: tunnel velocity, 0 to 75 m/s; inlet angle of attack, 0 to 120°; and fan face corrected airflow per unit area, 75 to 200 kg/s m^2. The inlet flow separation boundaries, the fan face total pressure recovery and distortion characteristics, and the fan blade vibratory stresses were determined. The recovery, distortion, and stress levels showed no abrupt changes at the onset of separation, but became gradually more unfavorable as the size and intensity of the separation increased as induced by increasingly severe operating conditions. Performance characteristics for a large scale model of the inlet were estimated from these test results.

17. Key Words (Suggested by Author(s))	18. Distribution Statement
Boundary Layer Fan Inlet Flow Separation V/STOL	

19. Security Classif. (of this report)	20. Security Classif. (of this page)	21. No. of Pages	22. Price*
Unclassified	Unclassified	58	

* For sale by the National Technical Information Service, Springfield, Virginia 22161

SUMMARY

An inlet model coupled to a .508 m tip diameter turbofan simulator was tested in the NASA-Lewis Research Center's 9-by 15-ft Low Speed Wind Tunnel. The model was designed to operate at high angle-of-attack conditions that would be encountered during vertical take-off and landing of a tilt nacelle airplane. Testing was conducted at freestream velocities of up to 75 m/s, angles of attack of up to 120°, and fan face corrected airflow rates per unit area of 75 to 200 kg/s m^2.

The inlet flow separation boundary was found to be a simple function of velocity ratio and angle of attack. The fan face total pressure distortion characteristics were shown to correlate with the flowrate where separation occurs. The fan could be operated safely well into the separated flow regime before blade stress limits were encountered.

Analysis of the inlet static pressures indicated the presence of a localized separation bubble in the diffuser prior to the occurence of separated flow at the fan face. Flow separation boundaries and distortion characteristics for a large scale model of the inlet were estimated from empirical relationships developed from the test results.

1. INTRODUCTION

Subsonic airplane engine inlets are generally subjected to the highest angles of attack during near-runway operation. On a tilt-nacelle V/STOL aircraft the propulsion pod is rotated to a vertical position during the vertical take-off and landing transitions, which greatly increases the angle of attack on the inlet. The objectives of the present test program were to define the operating envelope where a fixed geometry inlet with reasonable length for a tilt nacelle V/STOL airplane can provide total pressure recovery and distortion levels that are compatible with high-bypass turbofan engines, including versions with low pressure ratio variable pitch fans .

The work reported here, including the design, fabrication, and testing of the inlet model, and documentation of the test results, was funded by NASA-Lewis Research Center (contract number NAS3-20597). This work is part of an on-going inlet development program aimed at improving subsonic inlet design technology, and providing design information for a tilt-nacelle V/STOL inlet. The next phase in the program will be the testing of a large scale model of the inlet coupled to a low pressure ratio high-bypass variable pitch fan turbofan engine.

LIST OF SYMBOLS

A_o	Hilite (inlet entry plane) area = .2241 m^2
A_1	Inlet throat area = .1495 m^2
A_2	Fan face annulus area = .1598 m^2
c_f	Local skin friction coefficient
H_i	Boundary layer shape factor $= \dfrac{\int_o^\delta (1 - \frac{u}{ue})\, dy}{\int_o^\delta \frac{u}{ue} (1 - \frac{u}{ue})\, dy}$
N_n	Nominal fan speed
P_c	Cowl static pressure
P_p	Boundary layer rake pitot pressure
P_{TMAX}	Maximum total pressure measured at fan face
P_{TMIN}	Minimum total pressure measured at fan face
$\overline{P_{T2}}$	Area weighted average total pressure at fan face
P_{T_∞}	Freestream (tunnel) total pressure
R	Radius referenced to fan centerline
R_0	Inlet hilite radius referenced to fan centerline
R_1	Inlet throat radius referenced to fan centerline
R_2	Internal cowl radius at fan face = .2540 m
RMS	Root-mean-square average of the fluctuating component of the fan face total pressure as measured by a single probe
rpm	Revolutions per minute
s	Distance from inlet hilite along cowl surface

u	Local velocity in the boundary layer
u_e	Velocity at the edge of the boundary layer
V_1	Equivalent one dimensional velocity at throat
V_∞	Freestream (tunnel) velocity
W_{K2}	Fan face airflow corrected to sea-level standard conditions
W_{K2S}	Fan face corrected airflow at the onset of separation
x	Distance from inlet hilite along fan centerline
y	Normal distance to cowl wall
α	Inlet angle of attack
δ	Boundary layer thickness
δ^*	Boundary layer displacement thickness
θ	Inlet meridional angle
σ	Fan blade stress as a percentage of the maximum allowable stress
ϕ_s	Empirical flow separation index for inlet

2. TEST DESCRIPTION

2.1 Test Model

Inlet Design

Nominal operating conditions for a tilt-nacelle V/STOL airplane on landing approach are illustrated in figure 1a. The take-off transition would be accomplished at lower angles of attack than shown in the design envelope. The maximum corrected airflow per unit area at the fan face is 205 kg/s m^2. The minimum airflow during landing is approximately 75 kg/s m^2 at the higher forward speeds (beginning of transition) and approximately 125 kg/s m^2 at the lower forward speeds (near touch-down).

The model is shown schematically in figure 1.b. The design incorporates some unique features. A cross section taken in a radial plane at the upper (leeward during angle-of-attack operation) part of the inlet shows a fairly conventional cowl, while a similar cut at the lower (windward) part of the inlet reveals much thicker and blunter contours. The purpose of the asymmetry is to take advantage of the operating characteristics of the airplane; i.e., the inlet is subjected only to positive angles of attack. At a positive angle of attack the windward stagnation point moves outboard, increasing the internal pressure gradients, while the leeward stagnation point moves inboard reducing the internal pressure gradients. Thus for the windward cowl the operating condition becomes increasingly severe with angle of attack and freestream velocity. For the leeward cowl, the worst condition is ground static operation at maximum airflow.

Referenced to the fan centerline, the local contraction ratio $(R_0/R_1)^2$ for the leeward cowl is 1.30. This value is based on a review of the ground static performance of various existing inlets. For the windward cowl the local contraction ratio is 1.76. This latter value is based on results obtained from testing of a series of small scale axisymmetric inlet models, one of which is shown in figure 1.b. The overall area contraction ratio (A_0/A_1) for the asymmetric design is 1.50. The complete inlet contours are listed in table 1. Note that in cross section normal to the fan centerline the cowl contours are circular. Another feature of the cowl is that the wall curvature is everywhere continuous. This is considered important since near the cowl lip the flow attains transonic velocities at angle of attack, and potential flow analyses have indicated that at such velocities a continuous wall curvature distribution helps to maintain smooth pressure gradients.

The fan nose dome (spinner) used in the test was an existing piece of hardware. A new spinner was not required since the existing part (after repositioning) closely matched the contours of the spinner used with this cowl design previously (see reference 1).

Turbofan Simulator

A schematic of the turbofan simulator with the inlet is shown in figure 2. The fan is a single stage 50.8 cm diameter design which has a pressure ratio and tip speed representative of Type A V/STOL aircraft application. At the nominal design speed of 8020 rpm, the fan pressure ratio is approximately 1.17, and the tip speed is 213.5 m/s. At the maximum fan speed of 120 percent of the design value, the fan pressure ratio is 1.25 and the tip speed is 256 m/s.

The fan has 15 rotor blades and 25 stator blades with a rotor-stator spacing of approximately one rotor tip chord length. The rotor blades were fabricated from a titanium alloy and have circular arc airfoil sections.

The simulator has provisions for adjusting the fan blade pitch and hence has no midspan dampers. All test runs were conducted with the blades set at the design angle.

The fan is powered by a four stage turbine powered by high pressure, heated air delivered to the turbine through flow passages in the model support strut.

The fan exit nozzle area was sized to duplicate as closely as possible the operating line used in the previous inlet-engine test in the NASA-Ames full scale wind tunnel (ref. 1). The required nozzle exit area was .1598 m^2. The two operating lines are compared in figure 3.

A more complete description of the aerodynamic characteristics of the turbofan simulator can be found in reference 2.

Model Instrumentation

The model instrumentation is shown in figure 4.

Inlet instrumentation--The inlet had axial rows of surface static pressures located at three circumferential angles. The positions of the static taps are given in table 2. A total of 37 static taps were located in the windward plane to give a detailed description of the static pressure distribution. In addition, an axial row of 18 taps was located in a plane displaced 45 degrees from the windward plane, and a row of 12 taps was located in the leeward plane.

The inlet model had two six tube total pressure boundary-layer rakes which could be installed about midway in the diffuser of the inlet to determine the quality of the diffuser boundary-layer. The dimensions of the rakes are shown in figure 5. One of the rakes was located in a plane displaced 5 degrees from the windward plane (S/R_2 = 1.15) and the other was located in a plane displaced 50 degrees from the windward plane (S/R_2 = 1.13).

The fan face rake details are shown in figure 6. Each of the six equally spaced arms contained 19 total pressure probes. Six of the probes on each arm

were positioned to provide an equal area weighted measurement of the fan face flow while the remainder were positioned to provide a more detailed measurement of the outer surface boundary-layer and the mid channel flow. Six outer surface static pressure taps were located in the fan face plane and positioned midway between the fan face rakes (also shown in figure 6).

To detect the onset of internal flow separation in the inlet a miniature dynamic high response total pressure transducer was mounted in the fan face rake plane 2.79 cm from the outer surface and displaced 7.5 degrees from the windward plane (figure 4). The output of the transducer was filtered to remove the DC component of the signal, passed through an rms meter to provide an analog signal representative of the pressure fluctuation level, and then displayed online in the control room via an X Y plotter as a function of either fan speed or model angle-of-attack.

Turbofan simulator instrumentation--The nature of the flow at the fan stage exit (rotor and stator stages) was determined by five total pressure rakes with six tubes per rake located on an equal area weighted basis (figure 4). Each rake also had one total temperature probe located at roughly midspan of the flow passage. Surface static pressures were measured on both the inner and outer walls.

The fan blade vibratory stresses were measured using three strain gages located at the root on the suction side of the chosen blades at approximately the mid chord position. This position was responsive to all the blade vibrational modes and each strain gage was calibrated in terms of the maximum stress for each mode. All three gages were monitored during the test and essentially indicated identical readings. However for the purposes of data reduction and analysis, only one of three strain gage signals was employed.

2.2 Test Facility

Wind Tunnel

The test was conducted in the NASA-Lewis 9- by 15-ft Low Speed Wind Tunnel which is located in the return leg of the 8- by 6-ft Supersonic Wind Tunnel. A schematic of the facility is shown in figure 7. The test section operates at approximately atmospheric total pressure and has a free stream velocity range of 0-75 m/s.

A photograph of the model installed in the test section is shown in figure 8. The model rotates in a horizontal plane about a vertical support post which also provides passage for the high pressure turbine drive air. A portion of the adjacent wind tunnel vertical wall was removed to allow the fan and turbine exhaust flows to pass through the wind tunnel wall during the high angles-of-attack.

A more complete description of the aerodynamic characteristics of the Low Speed Wind Tunnel is given in reference 3.

Data Reduction System

The overall data reduction system is discussed in terms of the offline and online capabilities.

Offline data--The steady state static and total pressure measurements in the inlet and turbofan simulator and other variables such as temperatures within the simulator, fan speed, and inlet angle-of-attack were digitized and the information was stored on magnetic tape by the Lewis Central Automatic Digital Data Encoding (CADDE) system. A total of 495 data words were sampled during a data scan which took approximately 30 seconds to complete. The data were in turn sent to an IBM 360/67 computer and processed into the final engineering format.

Online data--Fan blade vibratory stress levels were continuously monitored during the test using a spectrum analyzer to provide a continuously updated stress spectrum which allowed the levels of the various stress modes to be observed. In addition, the output signal of the chosen strain gage was filtered at the frequency corresponding to the first flatwise bending mode and sent to the X Y plotter where the stress level could be displayed either as a function of fan rpm (or inlet weight flow) or model angle-of-attack.

In addition, all three raw blade strain gage signals were recorded on magnetic tape along with fan speed and angle-of-attack signals for post run analysis.

2.3 Test Procedures

A major concern during the test was the safety of the turbofan simulator. It was anticipated that at the extreme operating conditions (high free stream velocities and large angles-of-attack) fan blade vibratory stresses in excess of the limiting values could be encountered.

To ensure fan safety, the following test procedure was employed. Testing was initiated at operating conditions of low free stream velocities and angles-of-attack to minimize the levels of blade stress to be encountered. The operating conditions (free stream velocity and angle-of-attack) were established and as shown in fig. 9, the turbofan simulator speed was manually increased from a low rotational speed (ptA) which corresponds to a separated inlet flow condition to a higher speed (ptB) which corresponds to an attached inlet flow condition.

This sweep in fan speed was termed a safety sweep in that it determined the maximum fan blade stress levels to be encountered for the given operating conditions. The progress of a safety sweep was immediately stopped and fan speed reduced when limiting blade stress levels were approached. Fan blade stresses were monitored continuously during the tests to ensure that they remained below the operating limits.

Also, during a safety sweep a discrimination between separated and attached inlet flow could be made through an on-line monitoring of the levels of total pressure fluctuations as measured by the dynamic high response transducer.

Once the safety sweep was completed, the fan speed was slowly reduced until the dynamic transducer showed increased activity (ptC). A number of steady state data points were taken around this point of increased activity. The windward plane fan face rake profiles in this region were subsequently examined to determine the onset of separation.

Additional steady state data points were taken for reduced fan speeds (decreased inlet airflow) to document inlet/fan performance for increasing severity of separation (that is, the onset of separation moving progressively forward to the lip region of the inlet). Also data were taken for fan speeds greater than the speed corresponding to the onset of separation to document inlet/fan performance corresponding to fully attached boundary-layer flows.

This procedure was repeated for increased values of angle-of-attack for a given free stream velocity and then at increased free stream velocities to complete the desired matrix of operating conditions.

Model operating characteristics were also investigated for increasing angles-of-attack at constant inlet airflows. The desired inlet airflow was established by setting the fan speed to the required value, and the model was then increased in angle-of-attack until the dynamic transducer again showed increasing activity. A number of steady state data points were taken at angles-of-attack slightly above and below that angle corresponding to the increased dynamic transducer activity. In a similar manner, the windward plane fan face rake profiles were then compared to determine the actual onset of separation.

Online spectrum analysis of the fan blade unfiltered strain gage signals was performed to determine the modes of vibratory stress present. A typical spectral plot generated during the test is shown in figure 10. The plot shows a number of spectra of the fan blade strain gage signal generated during a sweep in fan speed from approximately 2000 to 8000 rpm. The various modes of vibration are indicated, and it can be seen that the only mode present is the first flatwise bending mode.

As already mentioned, fan blade vibratory stress characteristics were recorded using the online plots of the stress level as a function of fan speed which were generated for given operating conditions. A sample online stress plot generated during the test is shown in figure 11. The stress corresponding to the first flatwise bending mode is plotted in terms of the percentage of the limit value of stress and as a function of the fan speed.

In order to generate the online stress plots, the desired operating conditions were established and then after the safety sweep and acquisition of the pressure data, an automatic controller was used to uniformly increase fan speed from approximately 1000 to 9000 rpm. This procedure allowed a stress signature to be plotted which showed not only the levels for attached inlet flow but also for various degress of internal flow separation.

3. TEST RESULTS

3.1 Flow Separation Boundaries

Three aerodynamic indicators were available for detecting the presence of flow separation in the inlet. Viz.: the fan face rake total pressure profile, the boundary layer rake total pressure profile, and the fan face dynamic total pressure (Kulite) probe. Separation was induced by two methods: first, by reducing the fan speed (inlet airflow) at constant freestream velocity and inlet angle of attack, and second, by increasing the angle of attack at constant velocity and fan speed.

Based on test experience with similar small scale inlet models tested with a cold flow duct set-up (reference 1) it was expected that the Kulite probe would be the best indicator for the onset of separation. Abrupt changes in the turbulence level near the cowl wall had been experienced immediately following the boundary layer separation. Root-mean square averages of the fan face Kulite output are shown in Figure 12. When the separation occurs at a relatively low airflow (up to 100 kg/sm^2) the turbulence level increases rapidly thus providing a good definition of the onset of separation. However, when the separation occurs at a higher airflow a gradual increase in turbulence level is observed. The judgement as to whether the points represent attached or separated flow was therefore made on the basis of the fan face rake profiles. The flow is considered separated if the velocity gradient (du/dy) at the wall is zero or negative (filled symbols in Figure 12). If the indicated velocity gradient is very small the points are defined as incipient separation (flagged symbols). As may be seen the determination of the point of separation is somewhat subjective for the high airflow cases and probably falls within an error band of $\pm$2.5 kg/sm^2 or $\pm 2^o$.

It is believed that the gradual increase in turbulence level at the higher airflows is due to the dynamic pressure probe becoming immersed in the thickening boundary layer prior to the onset of separation, and a more rapid increase would be observed with a probe located farther from the cowl wall.

The readings, bracketing separation for the nominal airflows of 75, 100, 125, and 150 kg/sm^2 are shown again in figure 13. In this figure the freestream velocity and inlet airflow values have been combined into a single dimensionless parameter, the throat to freestream velocity ratio V_1/V_∞. Up to 90^o angle of attack and 150 kg/sm^2 airflow the separation boundary can be closely represented by the expression:

$$\frac{V_1}{V_\infty} = \frac{\sin\alpha}{c} - \cos\alpha$$

where c is a constant and can be thought of as the tangent of the angle (ϕ_S) included between the freestream and throat velocity vectors, as illustrated in the diagram in figure 13. For the solid curve in figure 13, ϕ_S has a value of 18.5^o. The experimental separation points for WK2/A2 = 175 kg/sm^2, and for $\alpha = 120^o$ fall to the right of the curve derived from the above equation. The value of this separation index (ϕ_S) is consistent with one obtained for a 38 cm inlet model tested previously without a fan, as described in reference 1.

The same inlet flow separation boundaries are shown in a different format in figure 14. The constant airflow contour lines were calculated from the solid portion of the curve in figure 13 for $\alpha<90^{o}$ and from the broken curve for $\alpha>90^{o}$.

3.2 Inlet Performance

Fan Face Total Pressure Distortion

The distortion, presented here, is defined as the difference between the maximum and minimum measured total pressure values divided by the area weighted average total pressure at the fan face. Radial total pressure profiles representative of headwind and severe angle-of-attack conditions are shown in figure 15. It is apparent from the figure that in all cases, except the two lowest airflow conditions at $\alpha = 60^{o}$ where large separations are present, the lowest total pressure values occur in the boundary layer near the cowl. Owing to the finite tip clearance of the fan rotor and the high blade velocity near the tip the fan efficiency is relatively low near the cowl. Thus losses in the flow close to the wall do not significantly affect the overall fan performance. Consequently, in the evaluation of flight hardware the flow contained in an annulus of some arbitrary height near the cowl is often ignored. This height is generally in the range of 1.5 to 2.5 cm full scale. Using this rule and the above method of calculating distortion it is evident from figure 15 that the distortion values calculated for the attached flow regime of the inlet depend strongly on how much of the outer flow one choses to ignore.

In this section two distortion parameters are presented. The first parameter will be called "97.5%-area distortion", and as the name suggests, was calculated by ignoring the outer 2.5% of the fan face annulus area. The purpose of calculating this parameter was to provide a basis for estimating the distortion characteristics of a large scale model of the inlet, which will be tested in the near future. The probes used in the calculation of the 97.5%-area distortion were selected to correspond to the large scale fan face rake configuration and are indicated by the small circles in figure 15. The second parameter will be referred to as the "91%-area distortion". For this calculation the outer 9% of fan face annulus area was ignored, which approximately corresponds to a 2.5 cm distance from the cowl wall on a full scale inlet. The 91%-area distortion values are shown to allow comparison of the present test results on a common basis with results from the testing of other inlets.

The 97.5%-area distortion values for five test runs are shown in figure 16. The runs were selected to allow comparison of distortion trends for various levels of separation airflows ($WK2_S/A_2$). It is apparent from figure 16 that the general levels of distortion increases with $WK2_S/A_2$. Also, in the attached flow regime all of the curves show trends that are similar to the baseline condition (case 0) where separation did not occur. In the separated regime, the distortion has local peaks for the more severe conditions. As the flow is reduced to very low levels (large separated volume) the distortion decreases for all cases. One of the most significant findings in the test is that the level of distortion remains relatively stable at the transition from attached

to separated flow, as illustrated by the closely grouped data points near the separation boundary in figure 16. The 91%-area distortion values for the same test conditions are shown in figure 17. The essential difference between the characteristics in figures 16 and 17 is that in the attached flow regime the 97.5%-area values increase with airflow while the corresponding 91%-area values remain at a lower level and are not significantly affected by the airflow. In the separated flow regime the two methods of calculation yield closer values. The reason for this can be easily seen in figure 15. When the flow is attached, the distortion values reflect the total pressure loss in the cowl boundary layer. Since the 91%-area calculation ignores more of the boundary layer, it yields lower distortion values for attached flow. When the flow separates, the size of the low total pressure region increases and influences the outermost probes used in both methods of calculation, and the distortion values are closer to one another.

It was noted in the discussion of figure 16 that the general level of distortion increases with the separation airflow, $WK2_S/A_2$. A study was made to determine whether the distortion characteristics of the inlet can be related simply to $WK2_S/A_2$. Four pairs of test runs were selected for the study, as illustrated in figure 18. For the two members of each pair flow separation occurs at approximately the same airflow rate, but at widely different freestream velocities and angles of attack. The 97.5%-area distortion characteristics for these runs are shown in figure 19. The correlation between the 97.5%-area distortion and separation airflow appears to be very good. The 91%-area distortion values for the same test conditions are shown in figure 20. Here the pairs of distortion curves do not lie quite as close to each other as in the previous figure, however the nominal level of distortion can still be correlated with $WK2_S/A_2$. That is; the difference between the characteristics for two members of the same pair is less than the difference between the average values for two pairs.

Extent of Separation and Total Pressure Recovery

Owing to the buildup of boundary layer on the internal cowl surface and the fan spinner, the fan face total pressure recovery must always be less than 100%. However; the flow contained in the boundary layer is a small fraction of the total fan face flow and at least part of the boundary layer is usually ignored (as discussed previously). The recovery values discussed below were calculated using the probes corresponding to the large scale rake configuration shown in figure 15. When the inlet flow is attached the recovery for the present inlet is always above 99%, and significant losses occur only when the flow separates.

Static pressure profiles at several airflow rates are shown for a typical operating condition in figure 21. In this figure the forward progress of the point of separation can be traced by noting the upstream end of a constant pressure region in the profile. (When flow separates away from a surface, the static pressure tends to remain constant over the affected region.) Also, since scanning of the data takes a finite time (on the order of a minute), and profiles in figure 21 indicate a uniform trend, it may be concluded that when

the test condition is kept constant the separation tends to remain stationary. The axial extent of separated flow developed from static pressure profiles for various test conditions and the corresponding recoveries are shown in figure 22. It is apparent from figure 22a that the separation always originates at a point well downstream of the minimum cowl radius (S/R_2 = .706) and gradually moves forward as the airflow is reduced. This characteristic implies that the separation-free operating range of the inlet could be increased through the use of active boundary-layer control, e.g. bleed.

When boundary layer control is used to prevent or delay separation, it must be applied upstream of the station where separation would occur without control. Thus if boundary layer bleed were provided near the minimum cowl radius, the separation airflow ($WK2_S/A_2$) could be reduced to at least to the level where the curves in figure 22a intersect the S/R_2 = .706 line. The amount of bleed required to accomplish this requires further analysis and testing.

The loss of recovery at the fan face becomes significant only when the separation moves close to the inlet hilite as illustrated in figure 22b. When the separation is contained downstream of the minimum cowl radius, the loss of recovery is nominal. Fan face recoveries for the test conditions, defined in figure 18, are shown in figure 23. It is seen in figure 23 that in the separated regime the recovery is lower at a given airflow rate when the separation occurred at a higher airflow. That is, a higher $WK2_S/A_2$ results in a lower recovery when separation occurs.

3.3 Fan Blade Stresses

Following the aerodynamic performance testing of the model, all instrumentation rakes were removed from the inlet and testing was resumed to evaluate the fan blade vibratory stresses. Data were obtained at various tunnel velocities and inlet angles-of-attack using the procedures described in section 2.3. The stress trace shown in figure 11 is typical of the results obtained in that four discrete stress peaks can be recognized. These peaks generally occurred in narrow fan speed ranges; the first between 3200 and 3500 rpm (engine order 7), the second between 3800 and 4000 rpm (engine order 6), the third at approximately 4650 rpm (engine order 5), and the fourth at approximately 5300 rpm (engine order 4). (A stress peak was also present at around 8200 rpm, however, the magnitude of this peak was not evaulated.

Since the peak stress always occurred at an rpm corresponding to one of the engine orders only the above mentioned fan speed values were considered in the analysis presented here. The stress maxima, as read from the on-line traces (e.g., figure 11) are summarized in figure 24. It is evident from the figure that the limiting stress occurred at the nominal fan speed of 4650 rpm at all of the conditions tested. It is also interesting to note that at the lower fan speeds (lower airflows) the stress increase to a certain value, then level off. At the highest tunnel speed (72m/s) the maximum tested angle-of-attack was 45°. This angle-of-attack was too low to cause an increase in any of the characteristic stress peaks.

One of the basic questions to be answered from the test was whether it is possible to run the fan safely when separated flow is present in the inlet. To illustrate the effects of inlet flow separation on the fan blade stresses, cross-plots of the stress data (figure 24) were superimposed on the inlet separation boundaries. These plots are shown in figure 25. It is evident from the figure that the separated flow regime can be deeply penetrated before excessive stresses occur in the fan blades. For instance consider the case at V_∞ = 34 m/s, $\alpha = 82^0$ at the nominal fan speed of 4650 rpm. (Recall that the absolute maximum stresses generally occur at N_η = 4650 rpm). According to figure 25, inlet flow separation occurs at this point. However, it is seen that at V_∞ = 34 m/s the angle-of-attack can be increased to 120^0, or at $\alpha = 82^0$ the tunnel velocity can be increased to 50 m/s before the 80% stress limit is reached. So in this particular case we could increase either the freestream velocity or the angle-of-attack by 50% beyond the point of separation without exceeding the fan blade stress limits. And we may conclude that, in general, the safe operating boundary of the fan is significantly higher than the inlet separation boundary.

4. BOUNDARY LAYER ANALYSIS

The inlet boundary layer development, near the onset of separation, was analyzed for selected test conditions to gain insight into the details of the separation phenomenon. The analysis was confined to the internal surface of the windward cowl, where separation generally originates. It was planned to use the results of this analysis to predict the performance of a large scale model of the inlet which will be tested in the near future.

4.1 Analytical Procedures

Measured Boundary Layers Profiles.

The Law-of-the-Wall/Law-of-the-Wake velocity profile representation has been generalized to include the effects of compressibility and pressure gradient in reference 4, where it is also demonstrated that this general form of the wall/wake profile agrees satisfactorily with experimental data for compressible turbulent boundary layers.

A least-squares-fit procedure was used to develop complete wall/wake profiles from the mid-diffuser boundary layer rake measurements obtained in the present test. The resulting profiles were integrated to determine the local skin friction coefficient, C_f, displacement thickness, δ^*, and profile shape factor, H_i. The shape factor is similar to the conventional shape factor parameter, displacement thickness/momentum thickness, except that in the calculation of H_i the density terms have been eliminated. Thus H_i is essentially independent of the edge Mach number and the wall temperature recovery and is a more useful indicator of profile distortion. For a "full" velocity profile (e.g. $u/u_e = (y/\delta)^{1/7}$) H_i has a value of 1.28, while $H_i > 1.8$ indicates a highly distorted profile. The calculations were carried out on a CDC 6600 computer using a program written for this type of data analysis. The program has been used previously with success in supersonic inlet work (reference 5).

Calculated Boundary Layer Profiles

The windward cowl boundary layer development was also calculated using the experimental surface static pressure distributions as inputs. This was accomplished with a compressible flow boundary layer program (reference 6) developed at Boeing. The program can solve axisymmetric problems, but assumes that the local boundary layer thickness is small with respect to the radius of curvature of the wall. In the present application the calculation was started by assuming a laminar boundary layer to originate near the stagnation point, the location of which was estimated by extrapolating the experimental static pressure distribution to $P_C/P_{T\infty} = 1.0$. The criteria for transition to turbulent flow must be input by the user. In the present work initially the transition point was assumed to be near to the minimum pressure point. (Since a laminar boundary layer tends to undergo transition when it encounters an adverse pressure gradient.) Review of the initial calculations indicated that the local Reynolds number, based on momentum thickness, usually had a value near 400 at the transition point defined in this way. Based on this, for ease of calculation, some of the later calculations were made by requiring

transition to occur when the momentum thickness Reynolds number reached 400 in the laminar boundary layer. When the specified criterion for transition is met the program switches from the laminar to the turbulent boundary layer equations. Since in a real flow the transition takes place over a finite distance, the computed flow properties in the immediate vicinity of transition are only approximate. However, this approximation has only a small effect on the properties calculated farther downstream. An eddy viscosity model of turbulence with the decay law is used in the program. This program has been shown to be accurate in the analysis of various supersonic inlet models (references 5 and 7).

If the calculated skin friction coefficient becomes zero, it is assumed that the flow separates and the computation is terminated. Thus, if in the real flow, a local separation exists with reattachment farther downstream, the boundary layer development can be computed only to the initial point of separation.

In the analysis the flow was assumed to be axisymmetric. Near the inlet entry plane the flow is three dimensional but the boundary layer is very thin. In the aft part of the diffuser where separation generally originates the circumferential velocity components tend to vanish. The same approach has been used successfully in the analysis presented in reference 1.

4.2 Comparison of Measured with Computed Profiles

The integral properties of the experimentally measured boundary layer profiles are summarized in figure 26. The freestream conditions presented here were the nominal design goals for the inlet. The parameters in figure 26 clearly indicate the increasing distortion of the boundary layer profile with decreasing airflow. It is also evident that separation ($c_f = 0$) is approached gradually. The flow separation boundary determined from the 5° mid-diffuser boundary layer rake data was found to be at slightly lower airflows than that determined from the fan face rake data. This again indicates that the separation originates well downstream in the diffuser, and gradually moves forward as the flow is reduced.

An attempt was made to calculate the boundary layer characteristics using the experimental cowl static pressure distributions as inputs as described in section 4.1. For conditions of completely attached flow, (generally at the higher airflow rates), the calculated profiles agree reasonably well with the measured values (see figure 27). However as separation is approached (lower airflows) the agreement becomes rather poor (see figure 28).

The static pressure profiles shown in figures 27 and 28 are shown again in figure 29 along with profiles for two intermediate attached conditions and a separated condition from the same run. Comparing the shapes of the profiles downstream of $S/R_2 = 1.0$ it may be noted that the curves for the three highest airflows have similar trends. The fan face rake data for the next lower airflow ($WK2/A_2 = 93$) indicates that the flow is attached; however, the static pressure profile of this condition, in figure 29, has a trend which is more

similar to that of the separated condition (WK_2/A_2 = 87 kg/sm^2) than to that of the remaining attached conditions. The aft portions of these profiles are shown enlarged in figure 30. The broken line in figure 30 was constructed by interpolation of data from reference 1, and is seen to be more in accord with the trend of the higher airflow curves than the actual data for WK_2/A_2 = 93 kg/sm^2. Both pressure profiles, i.e., the measured and constructed) for this data point were input to the boundary layer computer program. The resulting integral properties are shown in figure 31. For the actual pressure distribution the calculation indicated attached flow throughout the diffuser. When the modified pressure profile was input the analysis indicated separation at station S/R_2 = 1.30, i.e. only .15 R_2 downstream of the mid-diffuser boundary layer rake station. The integral properties obtained from the mid-diffuser rake data are illustrated by the filled circles in figure 31. The skin friction coefficient obtained from the rake data indicates that at the mid-diffuser rake station the boundary layer is very close to separation.

Based on the information presented in figures 29 through 31, the following hypothesis was developed. It is believed that the static pressure for WK_2/A_2 = 93 kg/sm^2 in figure 30 diverges from the normal trend (broken line) because the flow boundary was displaced by a local separation. The separation probably originated just downstream of mid-diffuser boundary layer rake but influenced the static pressure profile forward to $S/R_2 \approx 1.0$. If the above hypothesis is correct separation and reattachment must have taken place between S/R_2 = 1.15 and 1.76, (the location of the rakes).

It should be noted that only a minor modification was made to the actual pressure profile in figure 30 (the maximum change was approximately 1% P_{T_∞}), yet the modification resulted in significant changes in the predicted boundary layer properties as illustrated in figure 31. This indicates that a highly distorted boundary layer at low local Reynolds number (local velocity) is very sensitive to minor changes in the pressure distribution. Consequently an exact analytic prediction of the onset of separation is difficult.

According to the above hypothesis a local separation is encountered in the diffuser at somewhat higher airflows than those defined in Section 3.1. This separation starts out as a small bubble in the aft part of the diffuser and then slowly grows in both the forward and aft directions as the airflow is reduced. The separation boundaries presented in Section 3.1 correspond to the point where the separation is large enough to be sensed at the fan face rake station.

The presence of the separation bubble changes the static pressure profile in a favorable direction, i.e., the adverse pressure gradient decreases which results in an optimistic prediction of the boundary layer (see figure 31). As described in Section 2.3 a large number of data points were recorded near the onset of separation defined on-line by means of the fan face Kulite probe. These data points were to be used to predict the large scale inlet separation charateristics, which will be improved relative to the present model due to the higher Reynolds number. Because of the influence of the suspected local

separation on the static pressure profiles the calculation of the large scale boundary layer properties could not be carried out as planned. Instead, the flow separation boundaries for the large scale inlet were estimated by the procedure discussed in Section 5.1.

5. ESTIMATES FOR LARGE SCALE INLET

A large scale (R_2 = .70m) model of the inlet coupled to a high bypass turbofan was tested in the NASA-ARC 40- by 80-ft wind tunnel. The test was terminated prematurely due to a mechanical failure in the engine. However; some data were obtained prior to the failure. These results are reported in reference 1. It is planned to rerun the large scale test in late 1977. This section is concerned with estimating the performance characteristics of the large scale inlet on the basis of the present test results. The estimates are intended to allow for more efficient testing of the large scale model, and to validate the estimation procedures. It was planned to develop the large scale inlet separation boundaries from the small scale inlet static presure profiles (see section 4). As noted, that procedure was unsuccessful and the method described in section 5.1 was used instead.

5.1 Separation Boundaries

In section 3.1 it was shown that up to 90° angle of attack, and from 75 to 150 kg/s m^2 fan face corrected flow per unit area, the separation boundaries of the small scale inlet could be well represented by the empirical relationship:

$$(V_1/V_\infty)s = \frac{\sin \alpha}{c} - \cos \alpha$$

where $c = \tan 18.5^\circ$

This relationship is plotted in figure 32. We may reasonably assume that the full scale inlet separation boundaries can be represented by the same equation and an appropriate constant. In reference 1 it is reported that a single separation point was determined experimentally for the large scale inlet. This point is also shown in figure 32. The curve will pass through the experimental separation point for $c = \tan 22.4^\circ$. The separation boundary for the large scale inlet above 90° was drawn to follow the trend indicated by the small scale inlet curve.

The curve in figure 32 was expanded to yield the separation boundaries at constant corrected airflow for the large scale inlet as illustrated in figure 33. Results from the forthcoming test of the large scale inlet will be analyzed to evaluate the validity of the above procedure.

5.2 Fan Face Distortion

In section 3.2 it was shown that the fan face total pressure characteristics correlate well with the inlet separation air flow, $WK2_S/A_2$. On the basis of this finding it is hypothesized that the distortion characteristics of the large scale inlet can be estimated from the small scale results if allowances are made for the shifting of the separation boundary.

The 97.5-area distortion data shown in figure 16 were cross plotted against separation airflow at constant fan face corrected airflow. The faired curves

are shown in figure 34a. Thus figure 34a summarizes the inlet distortion characteristics; its use is illustrated in the following paragraph.

From the full scale curve in figure 32 we can calculate that at a freestream velocity of V_∞ = 40 m/s and angle of attack of $\alpha = 60^o$, the inlet flow will separate at a corrected airflow rate of $WK2\sqrt{\theta}/A_2$ = 69 kg/sm^2. We can then estimate the distortion curve for this condition (V_∞, α) by constructing a vertical line in figure 34a at $WK2\sqrt{\theta}/A_2$ = 69 kg/s m^2 and reading the values where the line intersects the curves. The curve in figure 34.b was drawn through the intersections. The data points in figure 34.b were obtained in the large scale inlet test at the above freestream conditions and a similar fan face rake configuration. The estimated curve shows surprisingly good agreement with the data.

The upcoming large scale inlet test will show whether the agreement holds throughout the test envelope.

6. CONCLUDING REMARKS

An approximately 1/3 scale inlet model designed for high angle-of-attack capability, coupled to a turbofan simulator, was tested at conditions representing near runway operation of a tilt nacelle V/STOL airplane.

- Operating conditions which result in the separation of the flow away from the internal surface of the windward cowl were determined. These conditions (freestream velocity, inlet angle of attack, inlet flowrate) could be reduced to a single curve of angle of attack versus inlet velocity ratio.

- The fan face total pressure distortion characteristics were found to correlate well with the airflow rate where separation occurred. Different combinations of freestream velocity and angle of attack had similar distortion characteristics when separation occurred at the same airflow.

- Fan blade stress maxima occurred at discrete narrow bands of fan speed. The safe operating limit for the fan was found to be well into the separated flow regime of the inlet.

- Integral properties of experimentally determined boundary layer profiles indicated that flow separation appears gradually and with adequate warning (e.g. increased turbulence near the fan face). Computation of the windward cowl boundary layer development near separation from the measured static pressure distributions was unsuccessful because of a suspected separation bubble in the aft region of the cowl.

- Flow separation boundaries for a large scale model of the inlet were estimated from the empirical relationship developed for the present model and a known separation point for the large scale inlet. Existing distortion data for the large scale inlet agreed with the distortion correlation developed here.

The results of the test indicate that a fixed geometry inlet is a viable candidate for application on a tilt-nacelle V/STOL airplane. The design technology acquired from continuing development of such inlets can also be applied to subsonic inlets operating in less demanding environment.

REFERENCES

1. Syberg, J. and J. L. Koncsek, Low Speed Tests of a Fixed Geometry Inlet for a Tilt Nacelle V/STOL Airplane NASA CR-151922, 1977.

2. Abbott, John M., James H. Diedrich, and Robert C. Williams, Low Speed Aerodynamic Performance of a 50.8 Centimeter - Diameter Noise Suppressing Inlets for the Quiet Clean Short Haul Experimental Engine (QCSEE) NASA TM X to be published.

3. Yuska, J. A., J. H. Diedrich, and N. Clugh, Lewis 9- by 15-Foot V/STOL Wind Tunnel NASA TM X-2305, 1971.

4. Paynter, G. C. and A. L. Schuehle, On the Use of Coles' Universal Wake Function for Compressible Turbulent Boundary Layers, D622755 TN, The Boeing Company, April 1969.

5. Syberg, J. and J. L. Koncsek, Experimental Evaluation of a Mach 3.5 Axisymmetric Inlet, NASA CR-2563, July 1975.

6. Reyhner, T. A., A Computer Program for Finite-Difference Calculation of Compressible Turbulent Boundary Layers, D6-23236, The Boeing Company, June 1970.

7. Syberg, J. and T. E. Hickcox, Design of a Bleed System for a Mach 3.5 Inlet, NASA CR-2187, January 1973.

Table 1. Inlet Contours

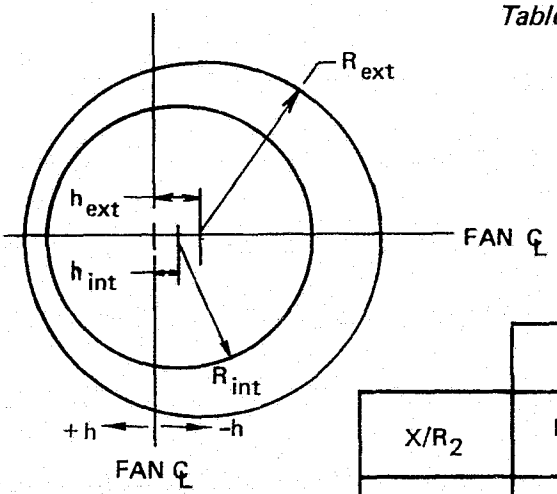

R_2 = .2540m, X = 0 at hilite

	External cowl		Internal cowl	
X/R_2	R_{ext}/R_2	h_{ext}/R_2	R_{int}/R_2	H_{int}/R_2
0	1.0514	-.0759	1.0514	-.0759
.0025	1.0700	-.0845	1.0316	-.0752
.0082	1.0848	-.0883	1.0160	-.0719
.0157	1.0971	-.0913	1.0023	-.0687
.0346	1.1172	-.0951	.9793	-.0632
.0535	1.1308	-.0968	.9622	-.0585
.0817	1.1460	-.0978	.9425	-.0528
.1100	1.1576	-.0978	.9269	-.0476
.1384	1.1672	-.0973	.9140	-.0429
.1667	1.1751	-.0964	.9032	-.0384
.2232	1.1882	-.0943	.8864	-.0301
.2799	1.1977	-.0925	.8748	-.0221
.3364	1.2084	-.0909	.8671	-.0144
.3931	1.2165	-.0896	.8622	-.0077
.4497	1.2237	-.0885	.8595	-.0019
.5063	1.2300	-.0875	.8588	.0031
.5629	1.2357	-.0867	.8601	.0073
.6195	1.2406	-.0860	.8632	.0106
.6761	1.2449	-.0855	.8680	.0131
.7327	1.2487	-.0849	.8742	.0148
.7839	1.2519	-.0845	.8816	.0158
.8459	1.2545	-.0842	.8901	.0162
.9591	1.2585	-.0837	.9093	.0155
1.0723	1.2605	-.0834	.9301	.0132
1.1463	1.2609	-.0833	.9439	.0112
1.1640			.9471	.0107
1.2731			.9659	.0073
1.3822			.9819	.0041
1.4913			.9937	.0015
1.6004			.9996	.0001
1.6368			1.0000	.0000

Spinner contours	
X/R_2	R/R_2
.8613	0.
.8863	.1120
.9113	.1440
.9613	.1970
1.0613	.2790
1.1613	.3380
1.2613	.3830
1.3613	.4200
1.4613	.4420
1.5613	.4530
1.6613	.4580
1.6368	.4600

Table 2. Inlet Static Pressure Instrumentation

Windward plane ($\theta = 0^o$)	$\theta = 45^o$	Leeward plane ($\theta = 180^o$)
$\frac{S}{R_2}$ = -.193	$\frac{S}{R_2}$ = -.188	$\frac{S}{R_2}$ = -.163
-.107	-.102	-.077
-.056	0.0	0.0
-.022	.056	.050
0.0	.112	.147
.013	.168	.226
.031	.224	.344
.051	.280	.490
.073	.336	.641
.099	.392	.861
.120	.448	1.082
.158	.504	1.413
.192	.560	
.237	.616	
.281	.672	
.321	.913	
.361	1.134	
.400	1.467	
.452		
.503		
.555		
.605		
.655		
.706		
.778		
.851		
.925		
.998		
1.072		
1.147		
1.230		
1.314		
1.397		
1.480		
1.559		
1.637		
1.716		

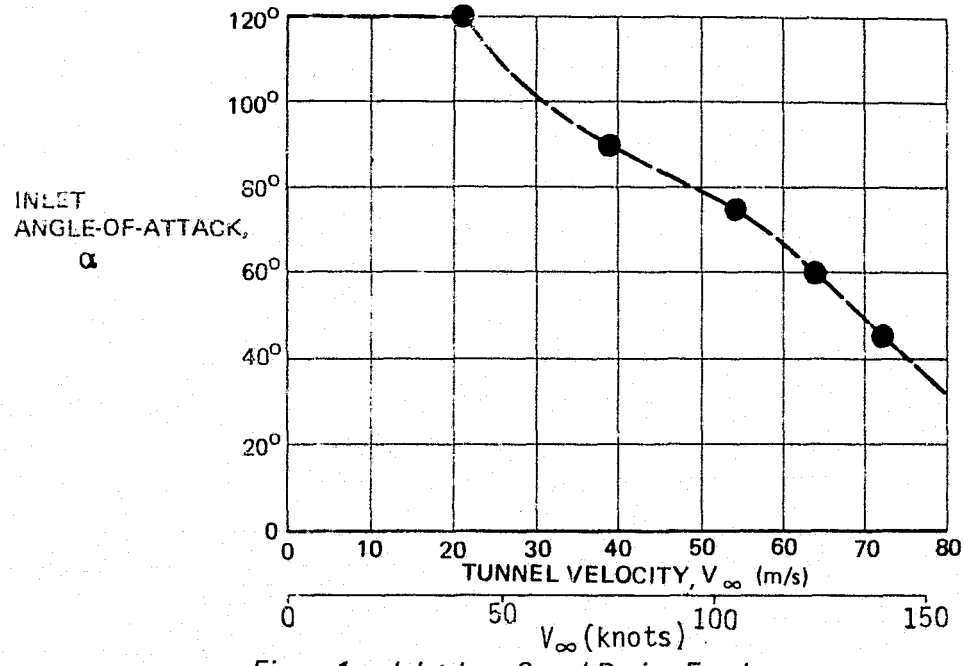

Figure 1a. Inlet Low Speed Design Envelope

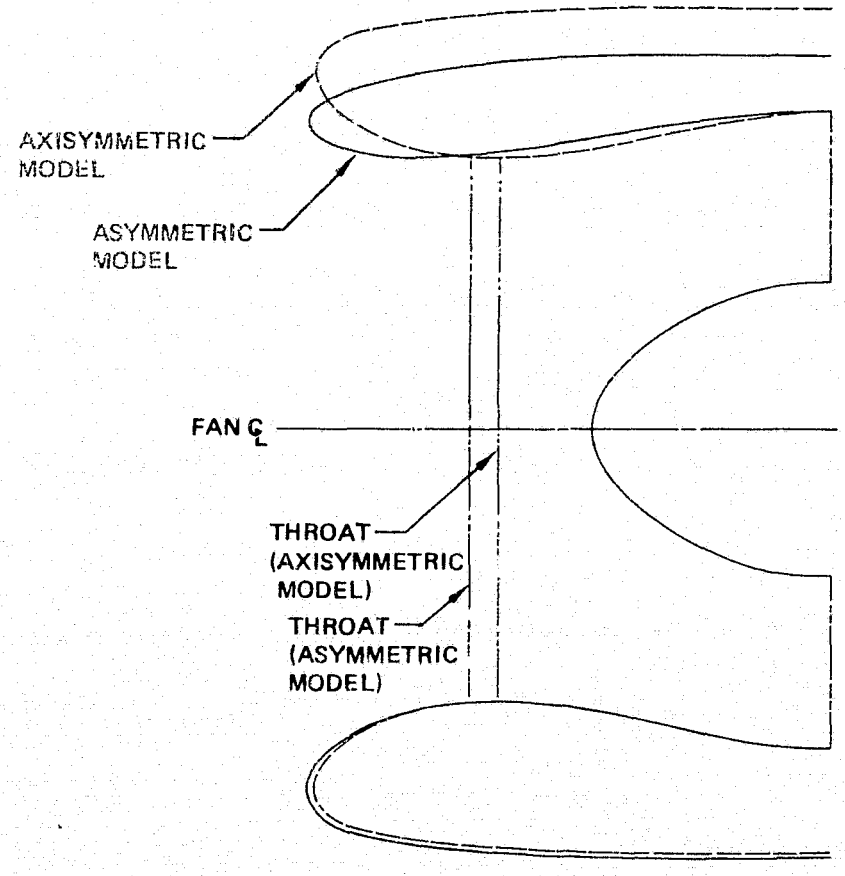

Figure 1b. Inlet Schematic

Figure 1. Inlet Design Goals and Model Schematic

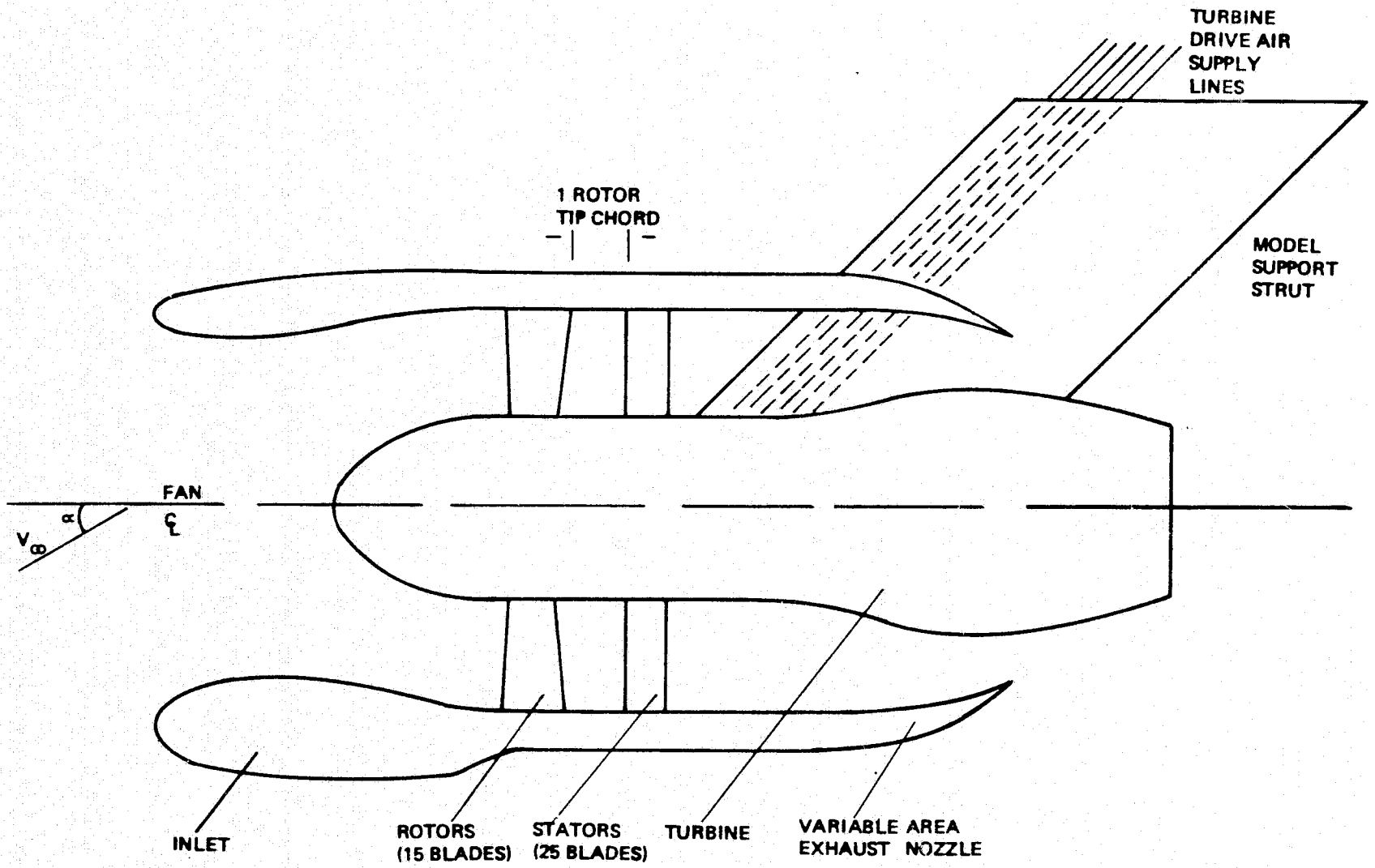

Figure 2. Inlet/Turbofan Simulator Assembly

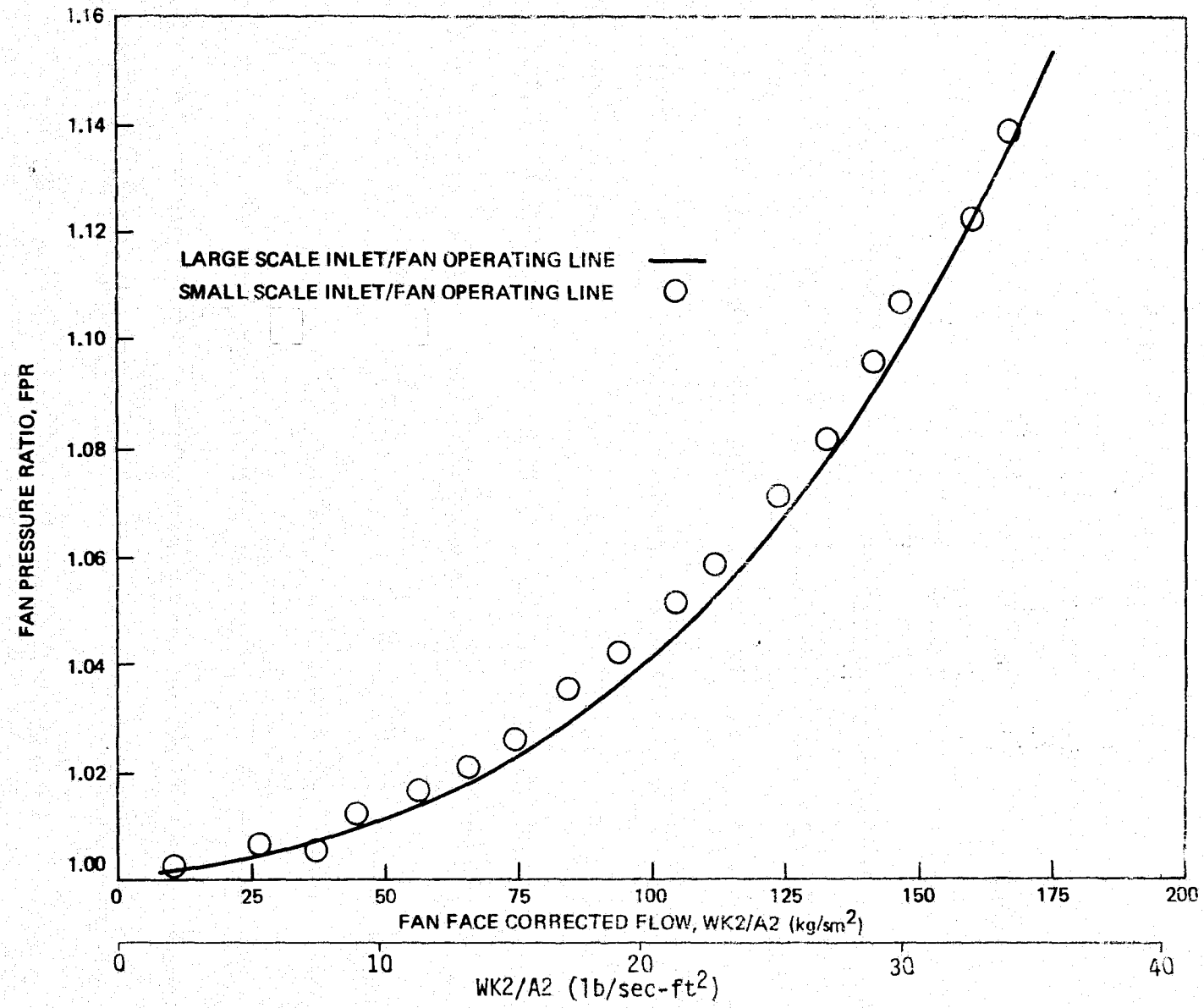

Figure 3. Comparison of Large Scale and Small Scale Inlet/Fan Operating Lines

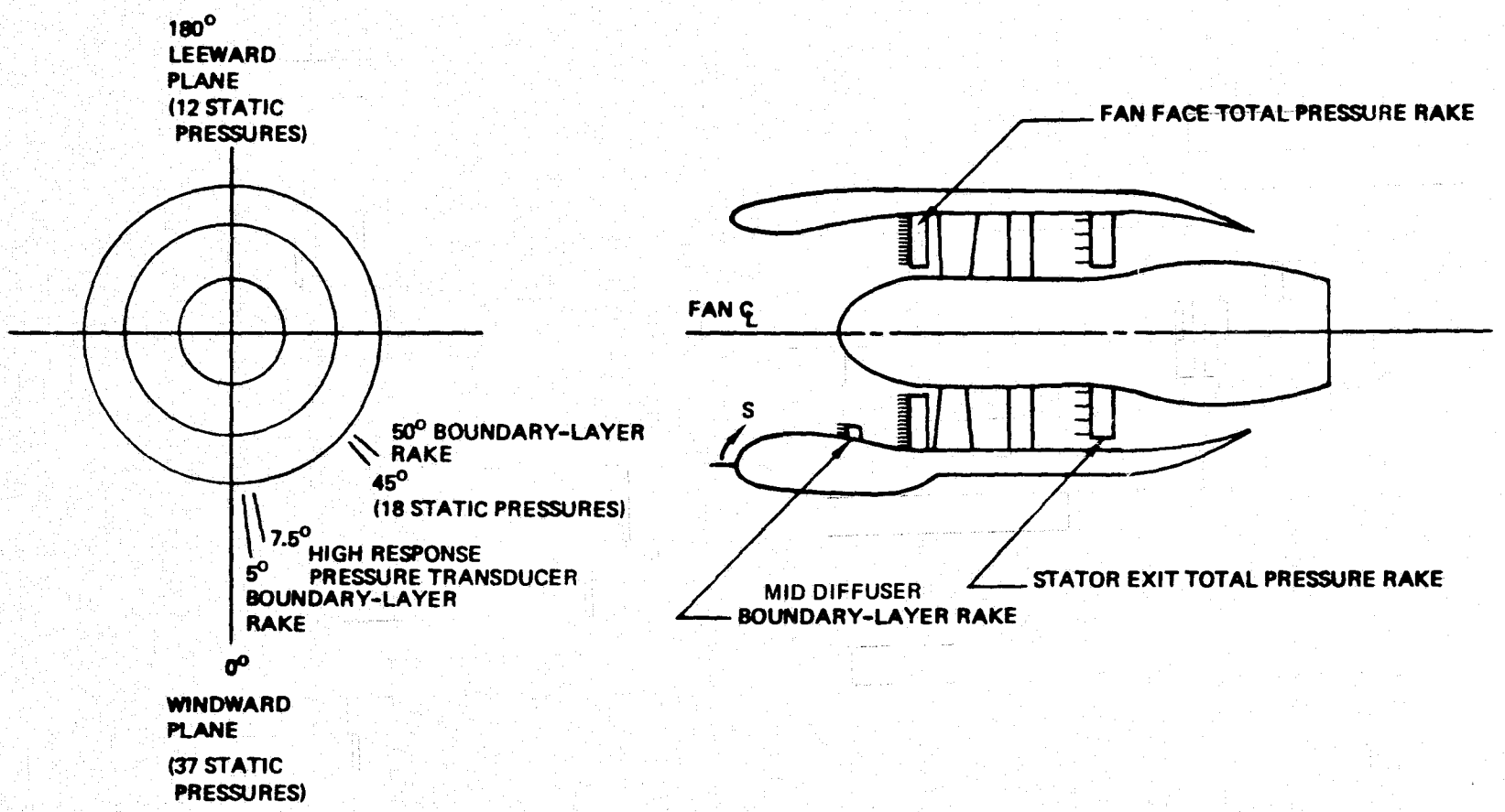

Figure 4. Instrumentation Locations

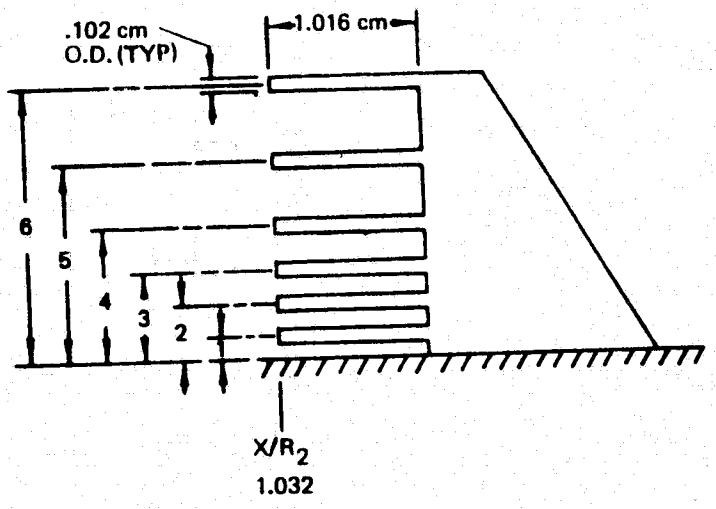

Probe No.	Design height Y/R_2	Measured height	
		5^o	50^o
1	.006	.008	.006
2	.015	.017	.014
3	.024	.025	.025
4	.036	.036	.036
5	.054	.055	.055
6	.075	.075	.073

Figure 5. Mid-Diffuser Boundary Layer Total Pressure Rake

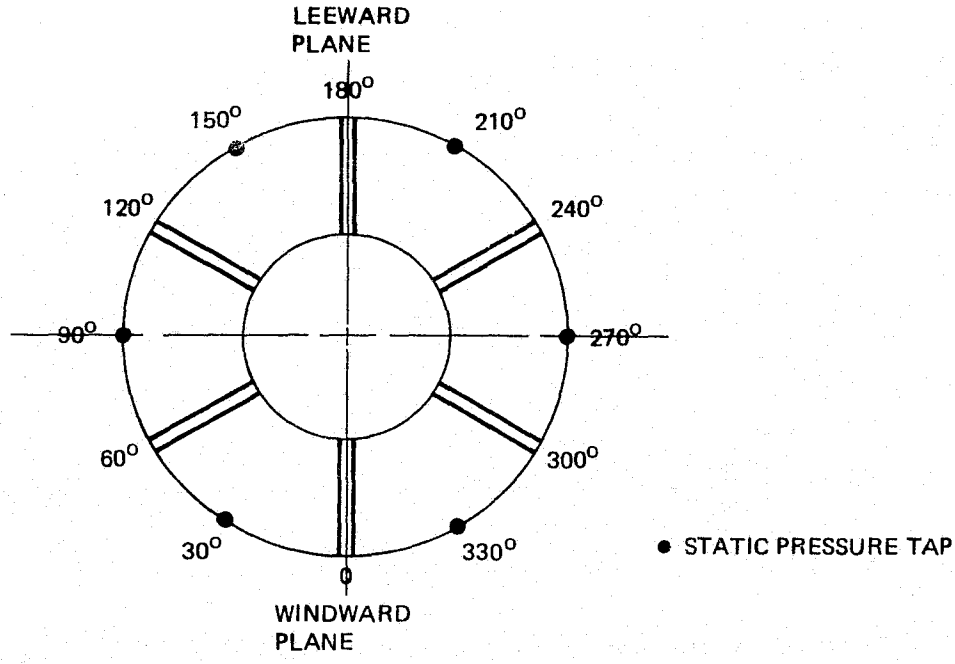

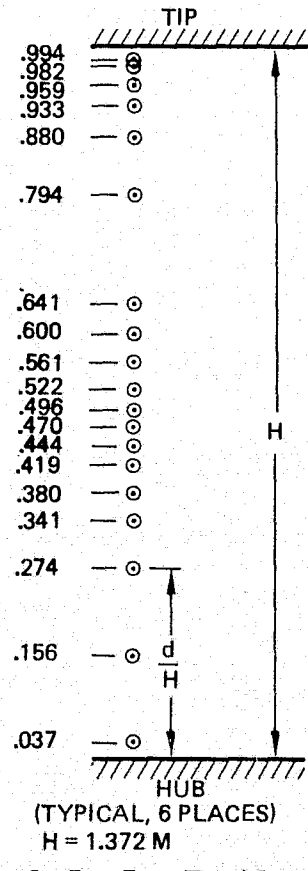

Figure 6. Fan Face Total Pressure Rake

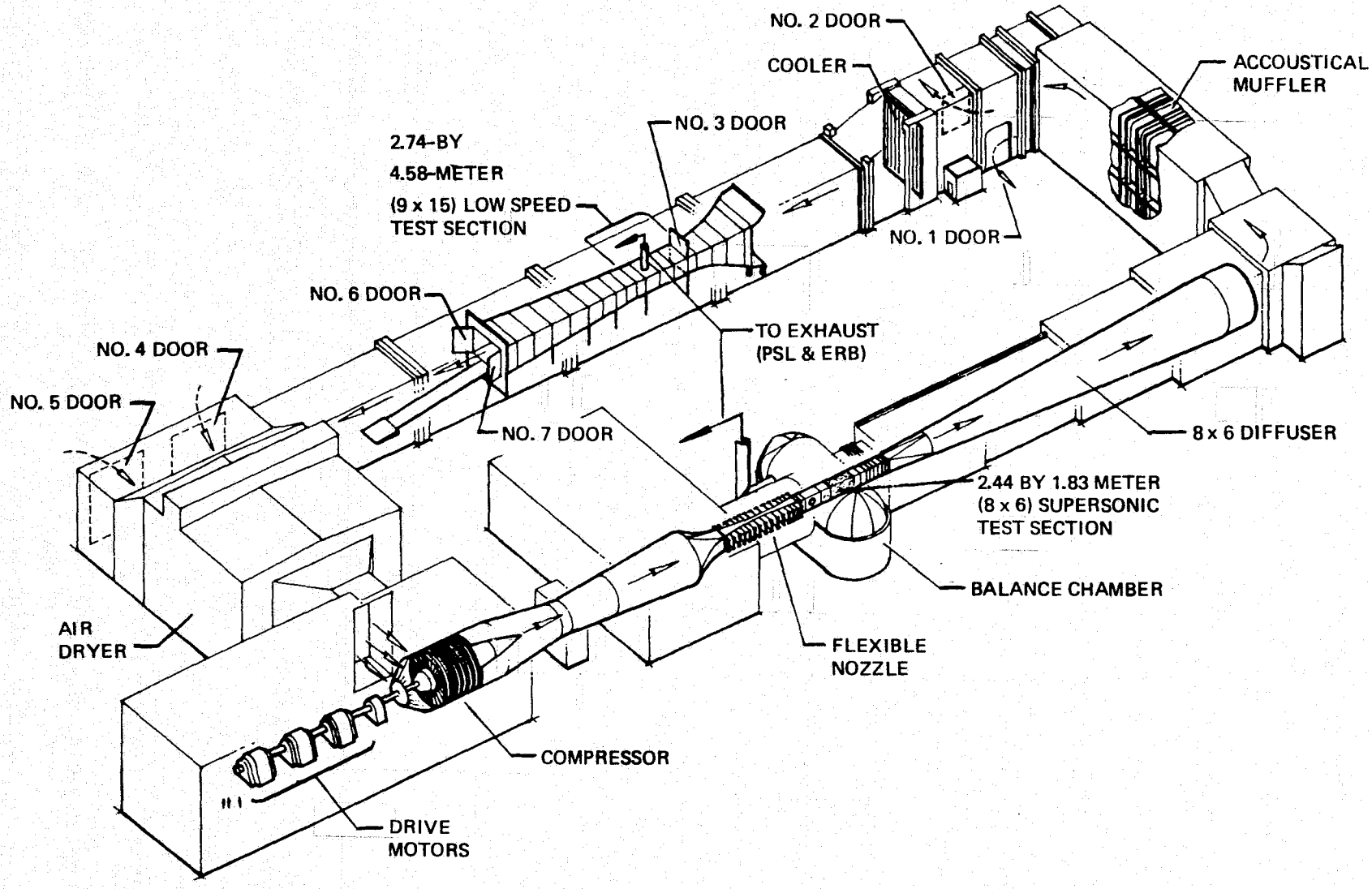

Figure 7. The NASA Lewis 8- by 6-ft Supersonic and 9- by 15-ft Low Speed Wind Tunnels

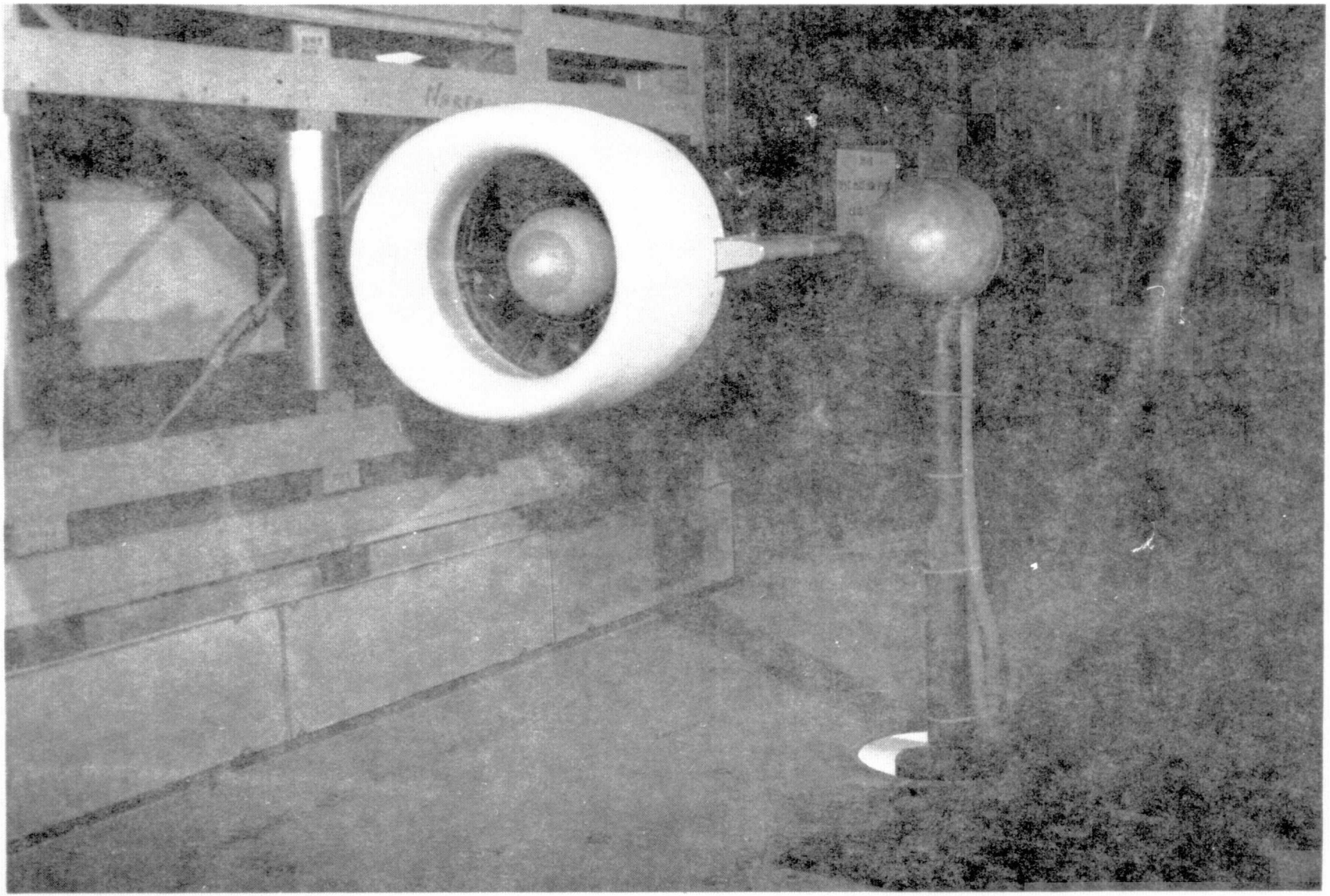

Figure 8. Inlet/Turbofan Simulator Assembly in Low Speed Wind Tunnel

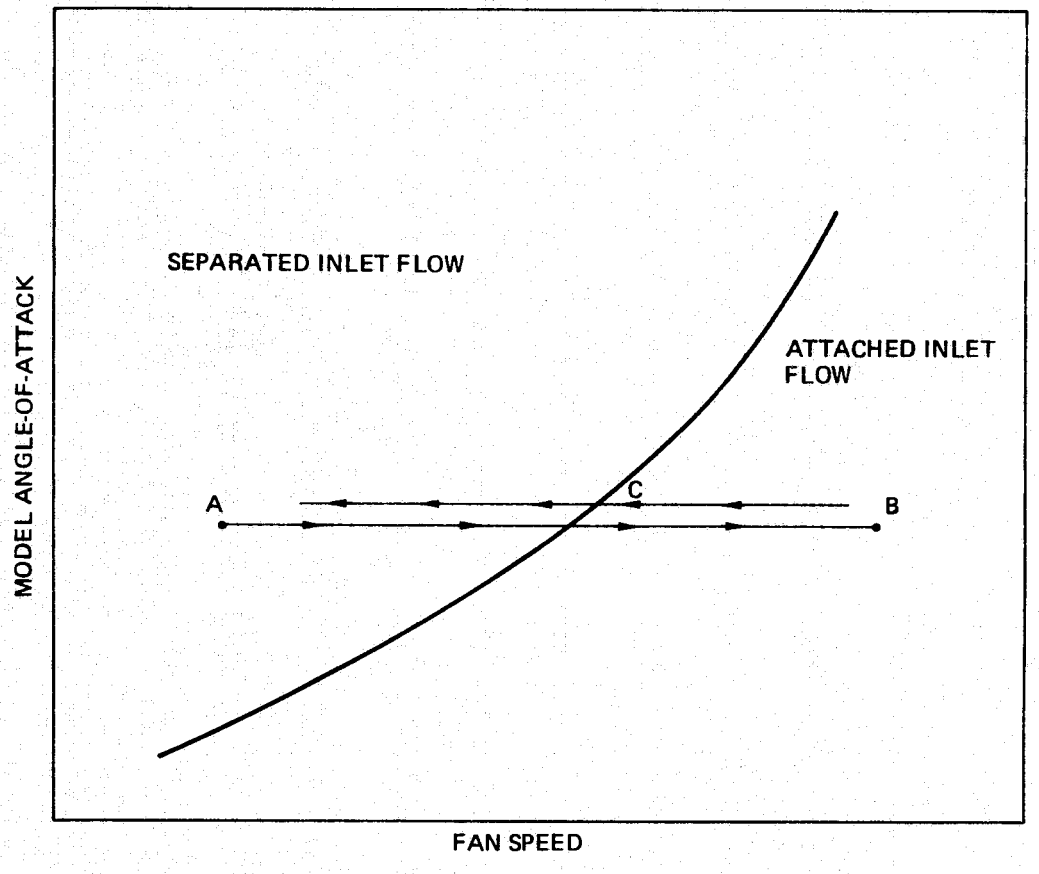

Figure 9. Data Acquisition Procedure

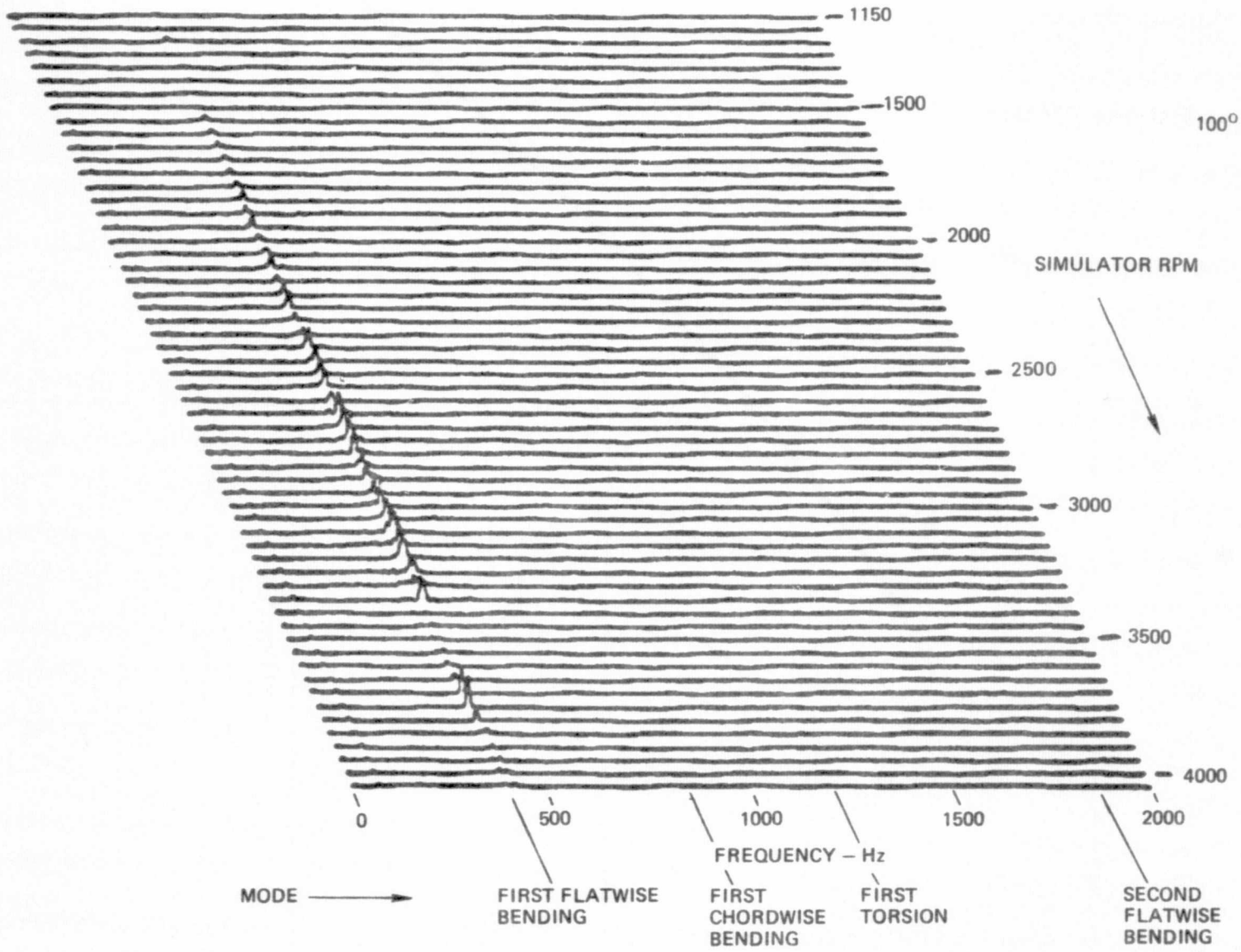

Figure 10. Typical Three Dimensional Spectral Plot

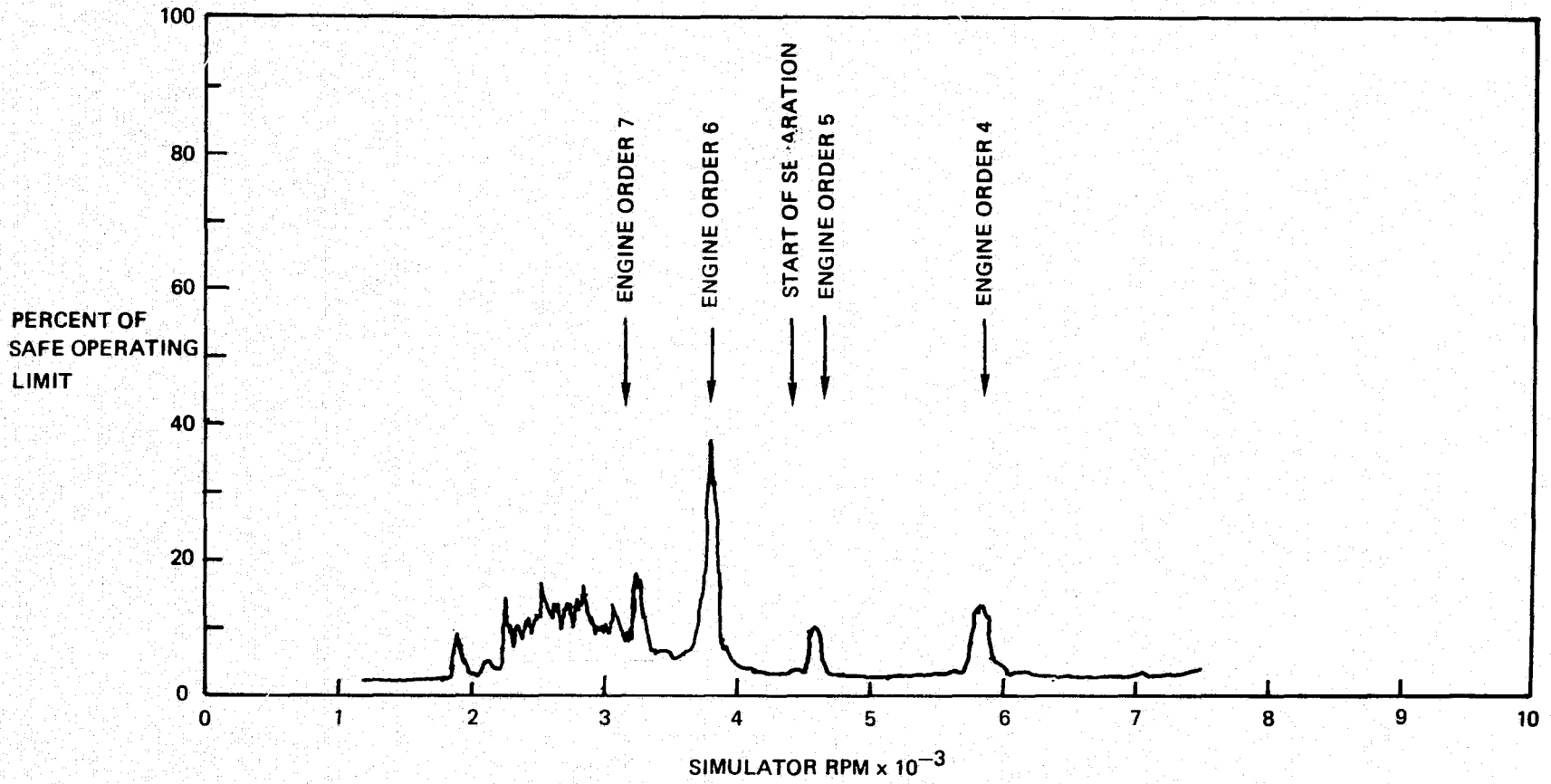

Figure 11. Typical Fan Blade Vibratory Stress Variation (First Flatwise Bending Mode)

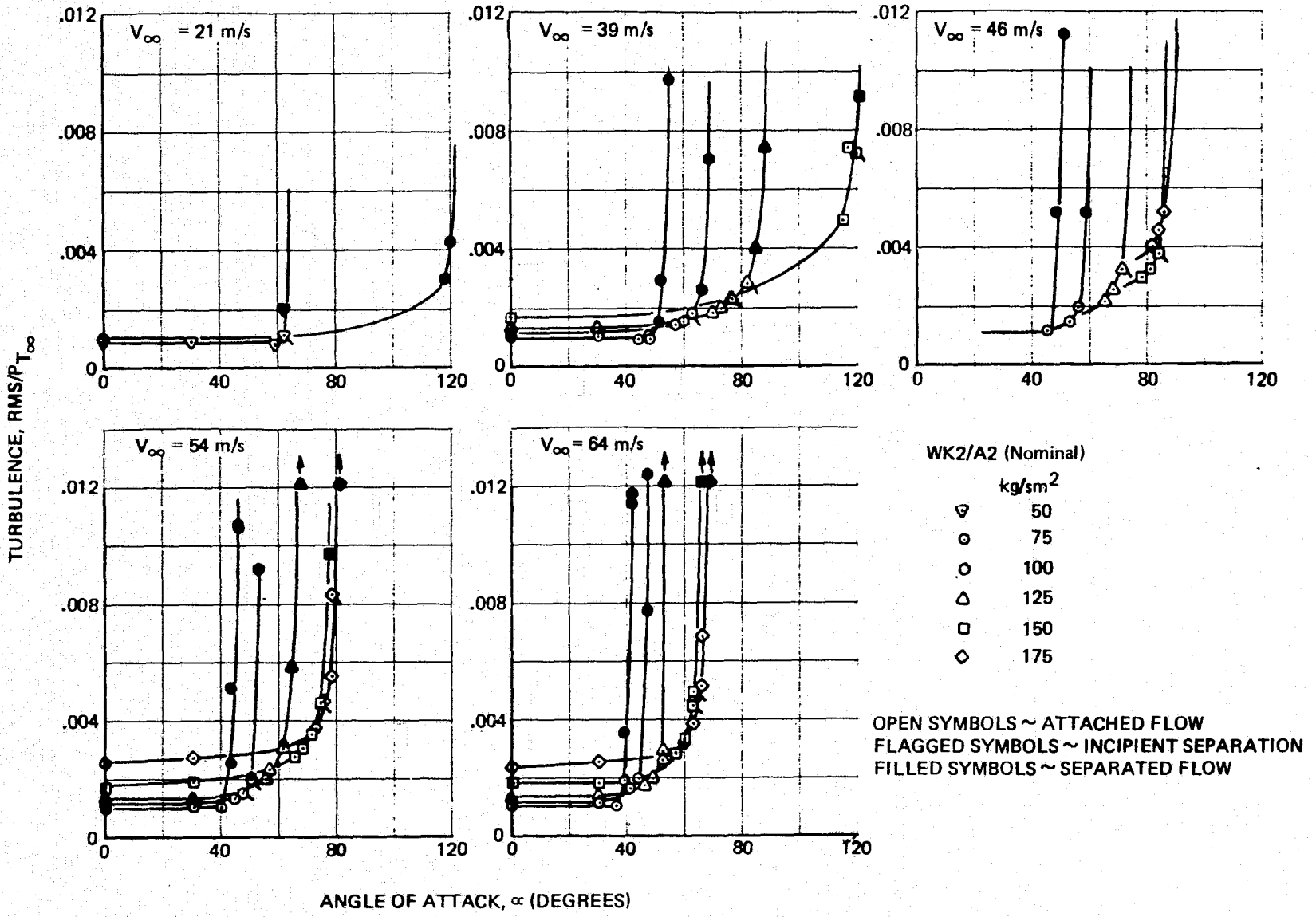

Figure 12. Dynamic Pressure RMS Averages Near Separation

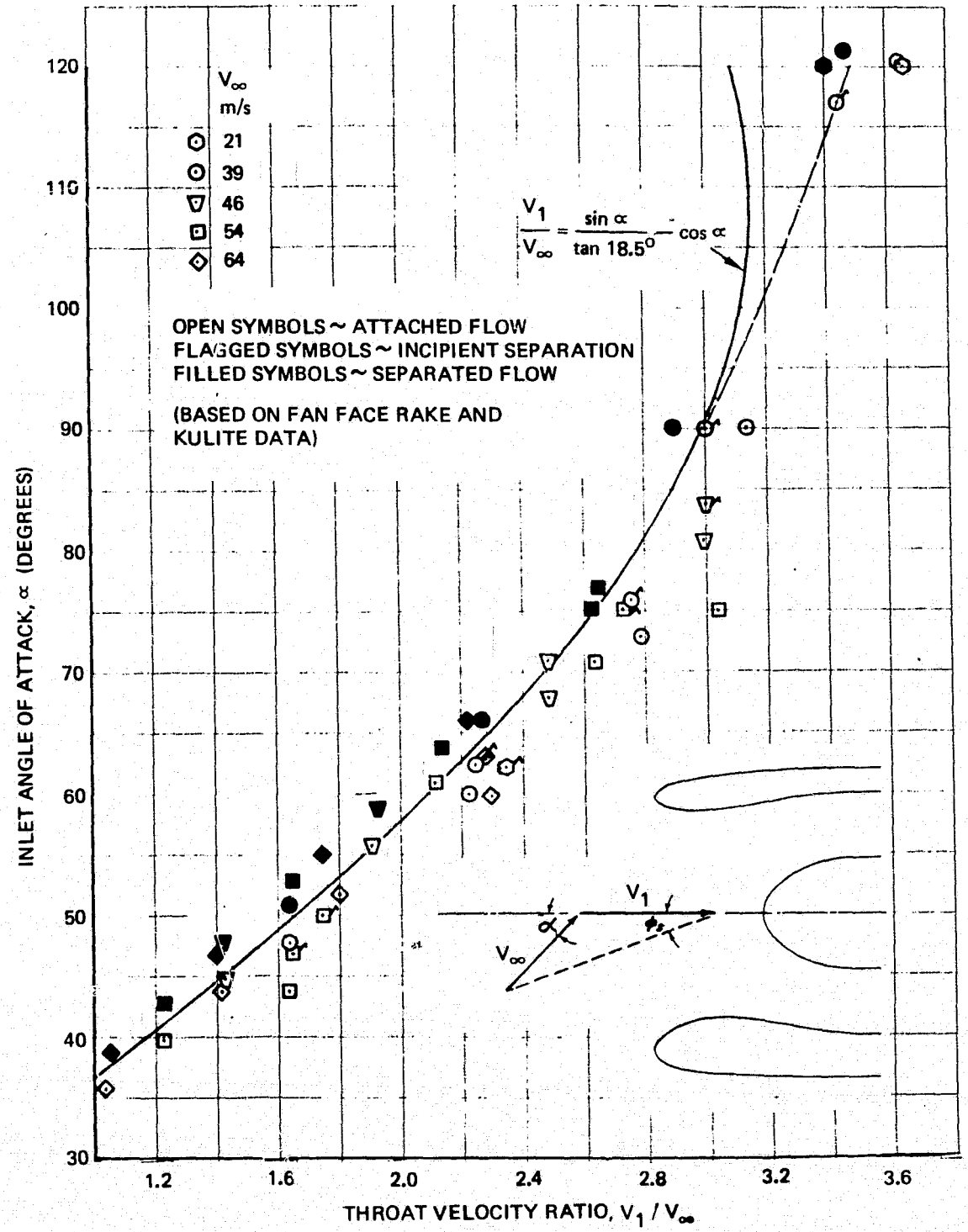

Figure 13. Inlet Flow Separation Boundary

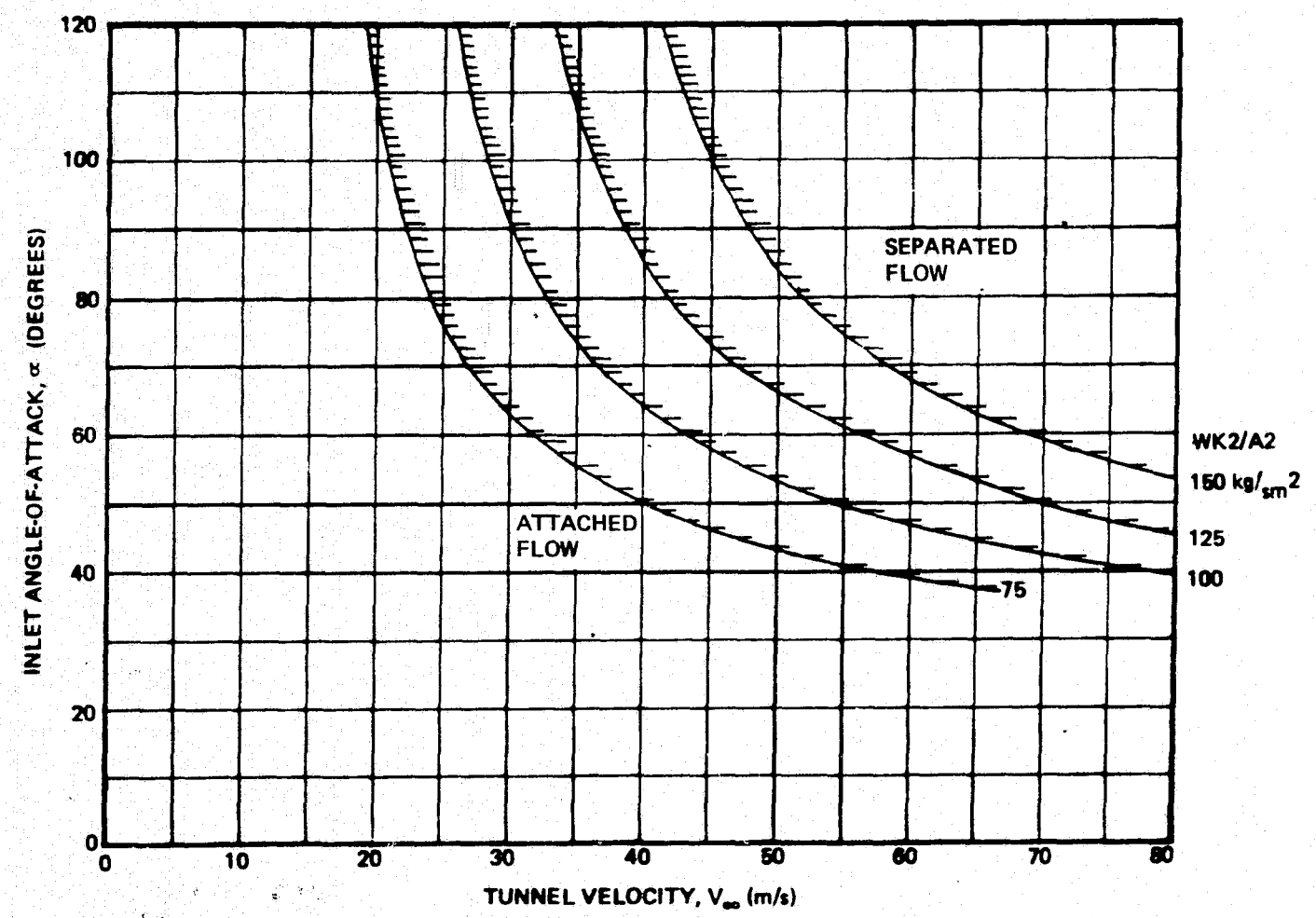

Figure 14. Inlet Flow Separation Boundaries for Constant Airflow

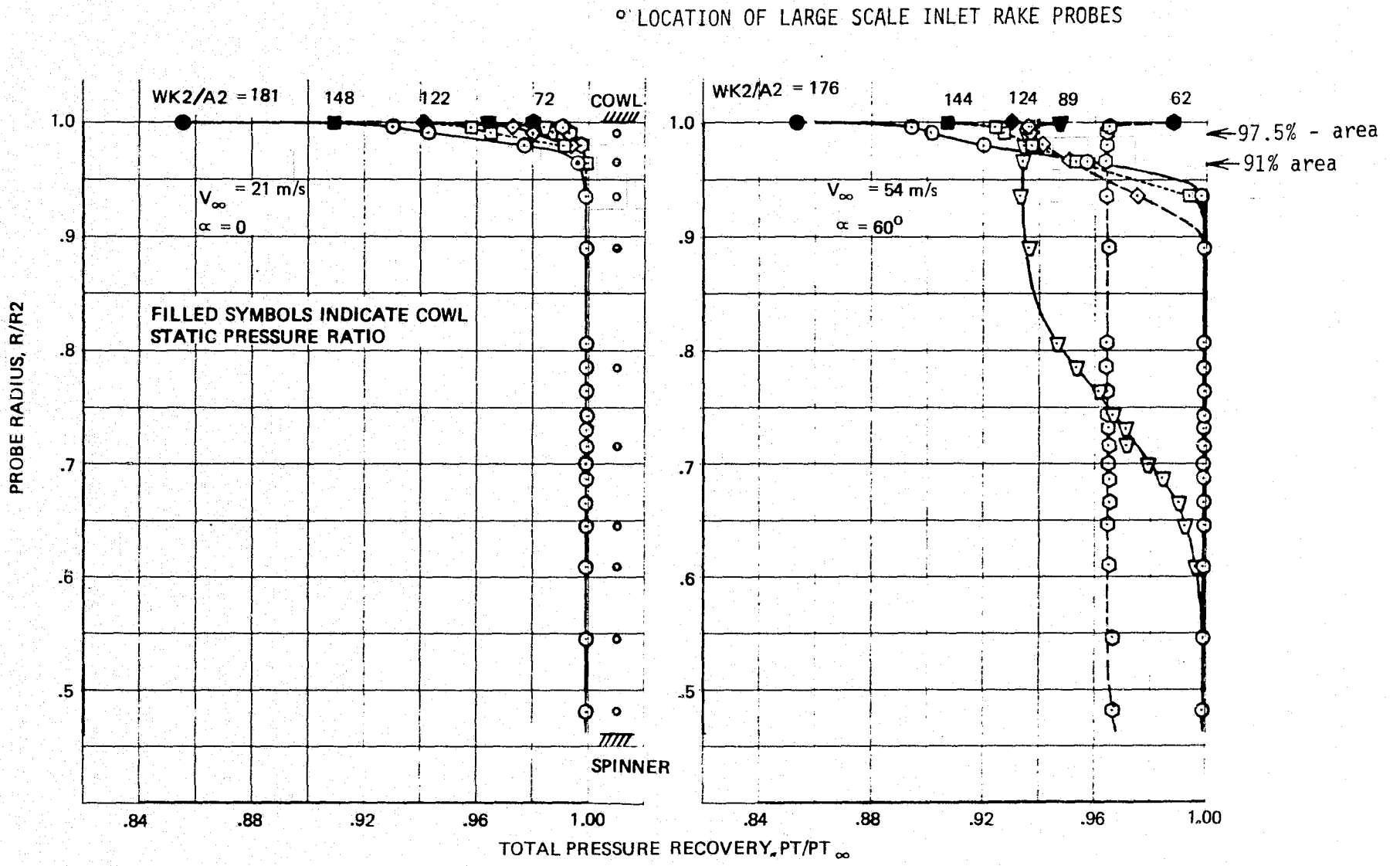

Figure 15. Fan Face Rake Total Pressure Profiles, Windward Side.

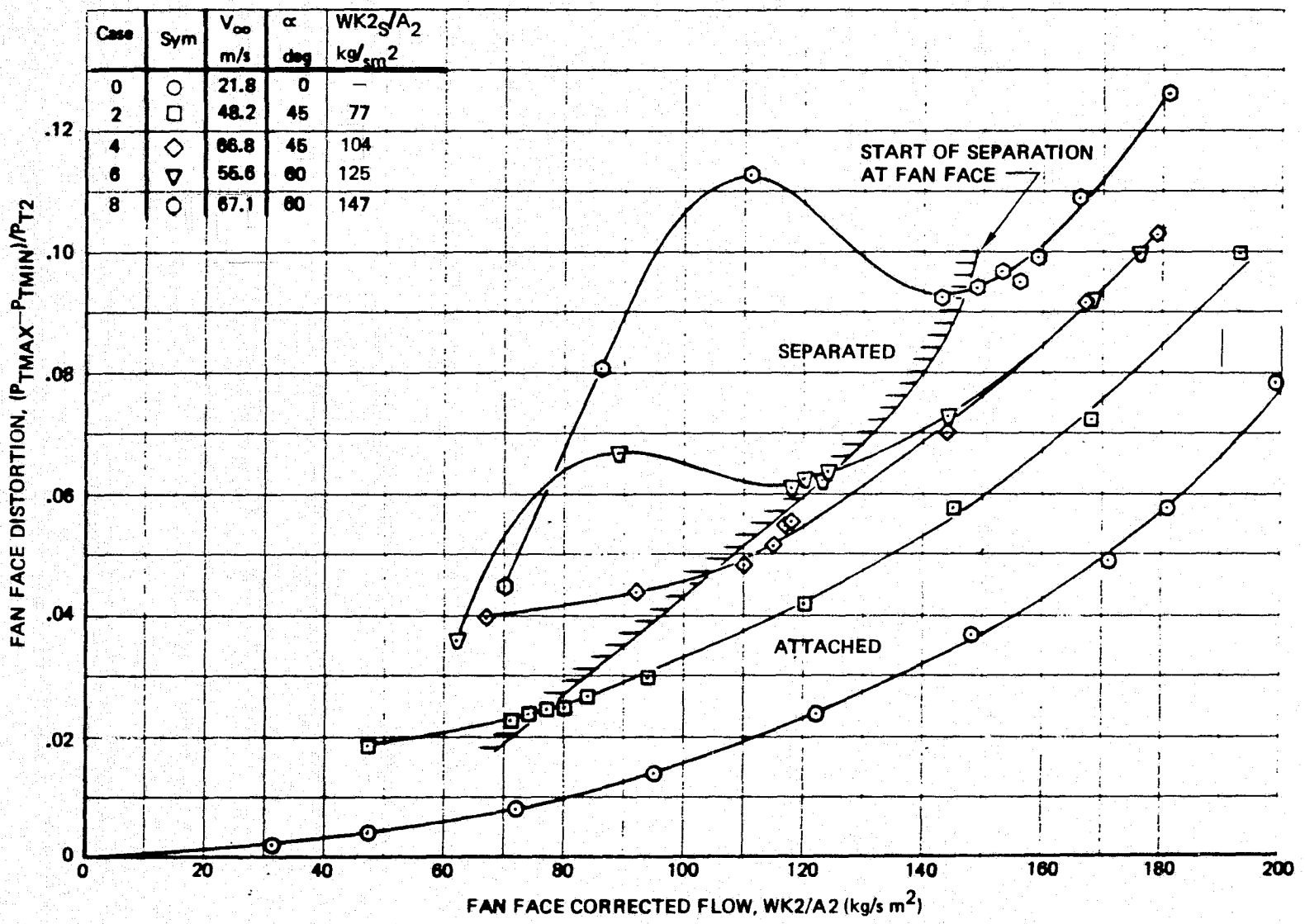

Figure 16. 97.5%–Area Distortion Characteristics

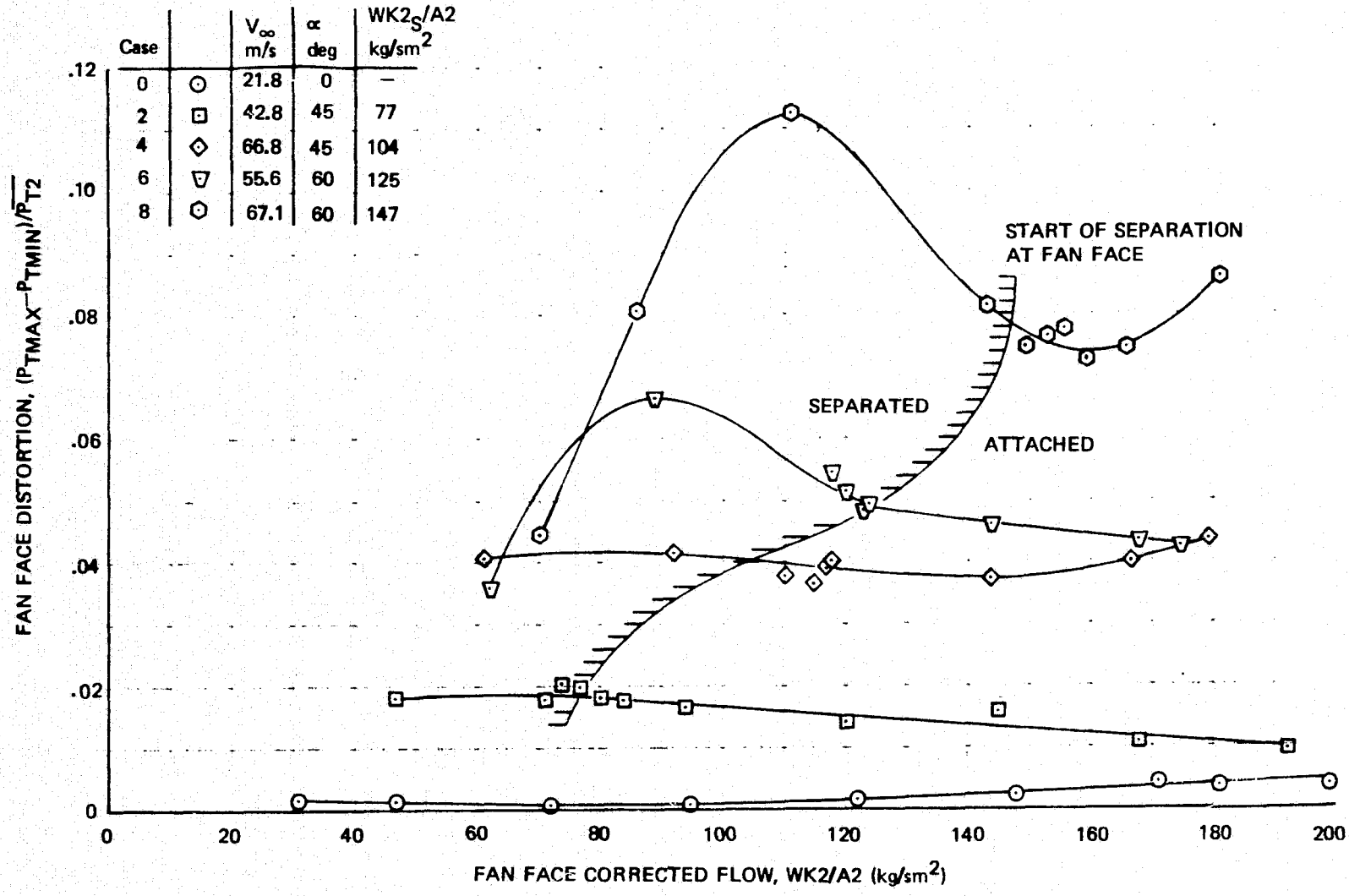

Figure 17. 91%—Area Distortion Characteristics

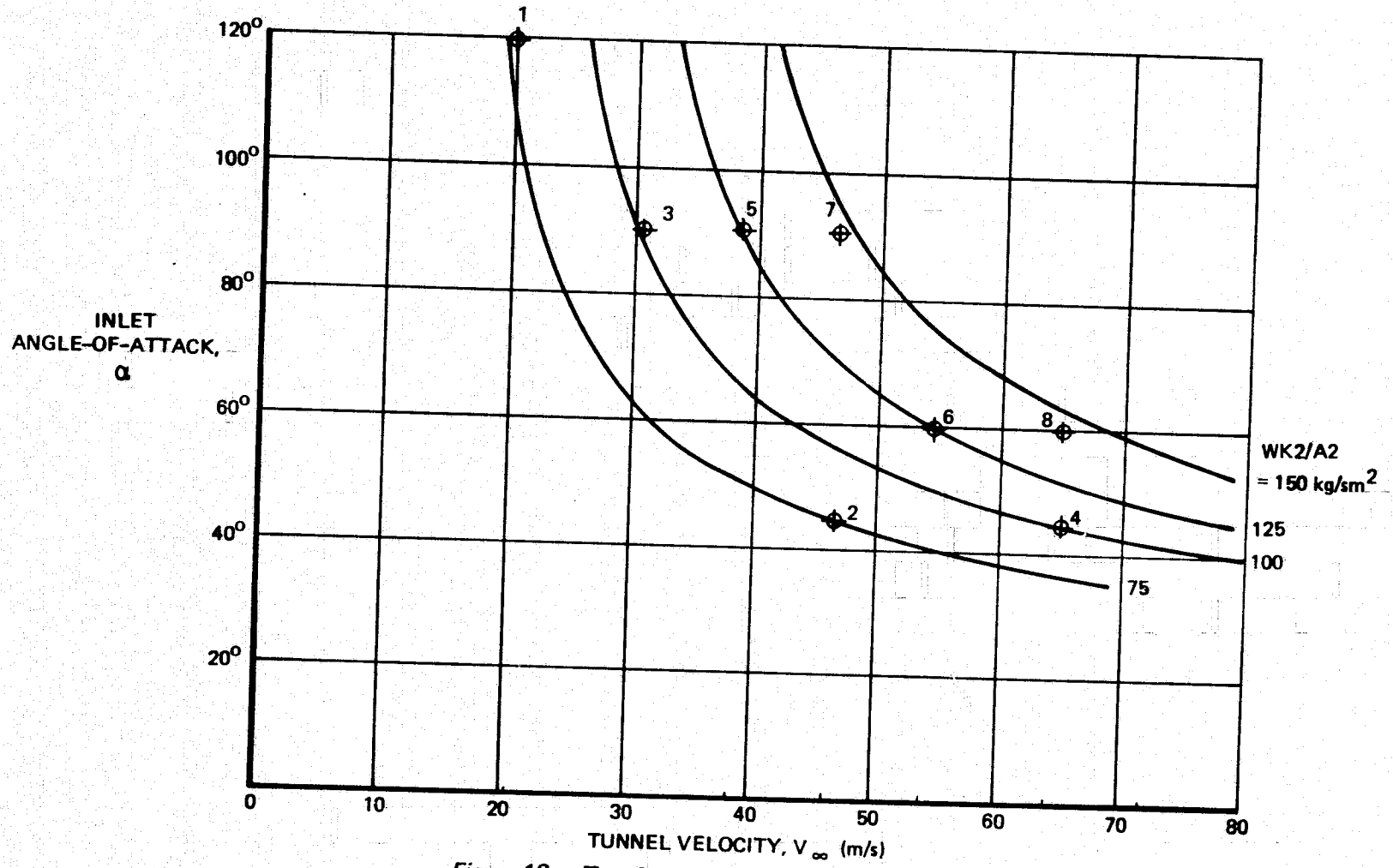

Figure 18. Test Conditions for Distortion Correlation

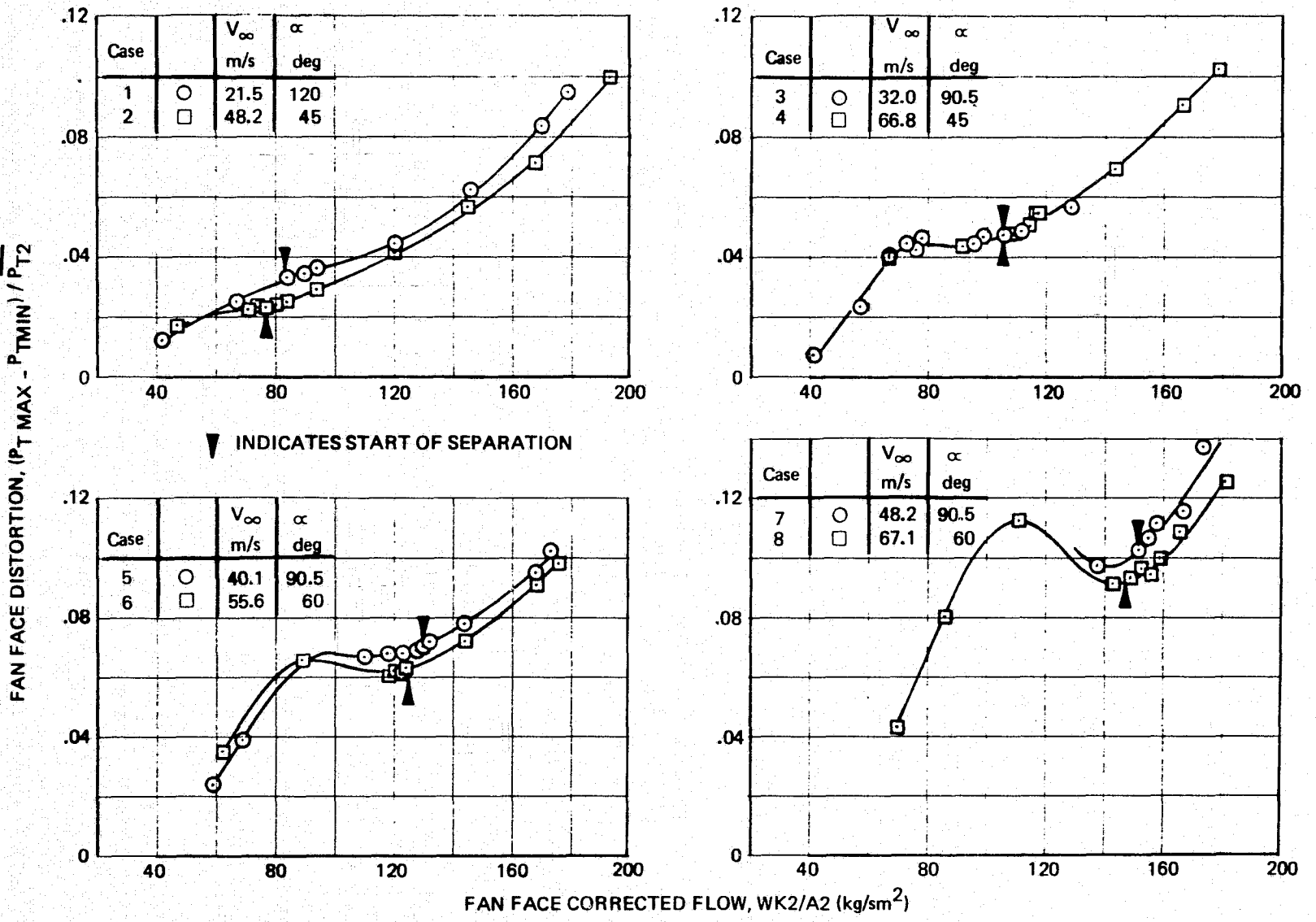

Figure 19. 97.5%—Area Distortion Correlation

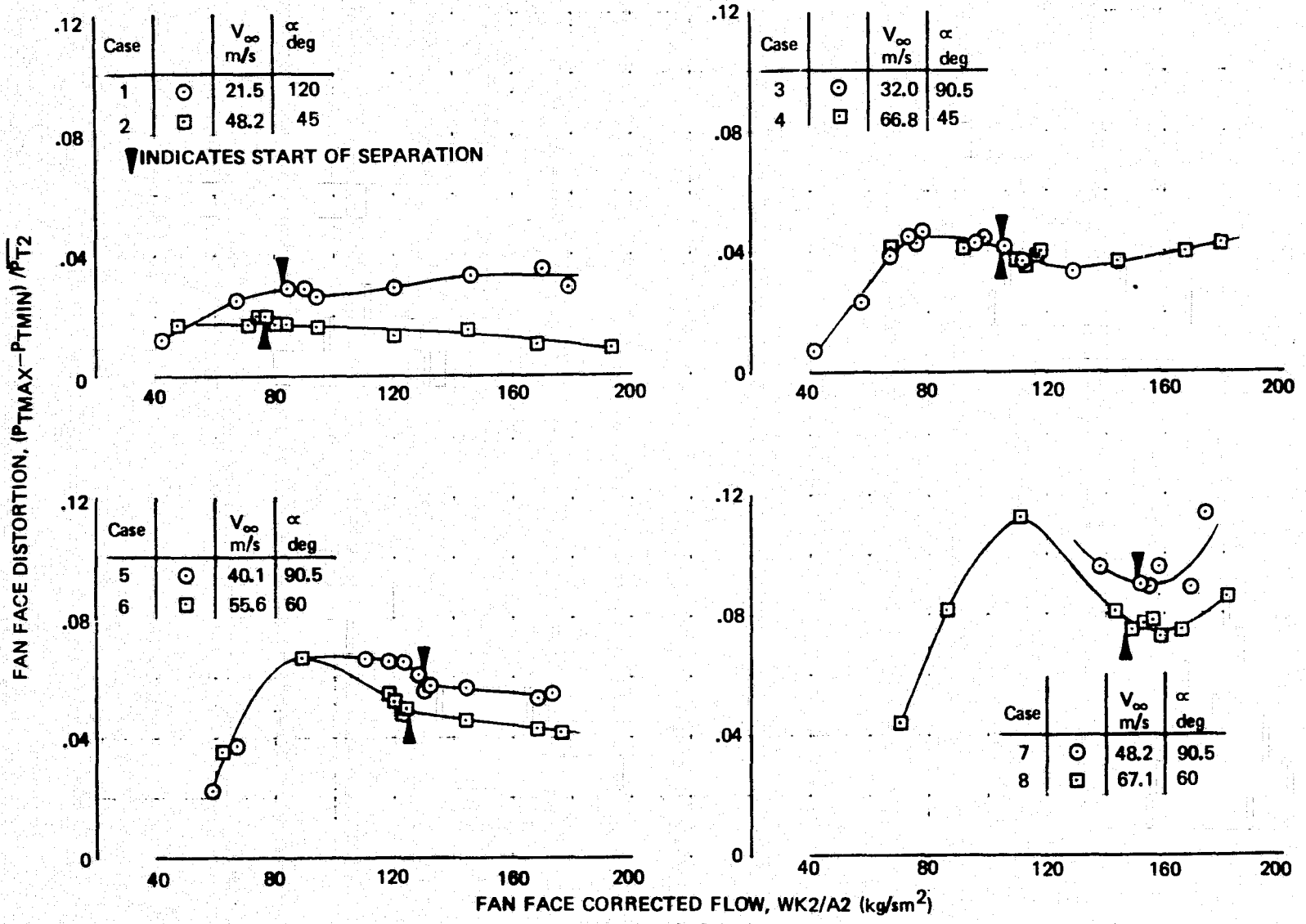

Figure 20. 91%–Area Distortion Comparison

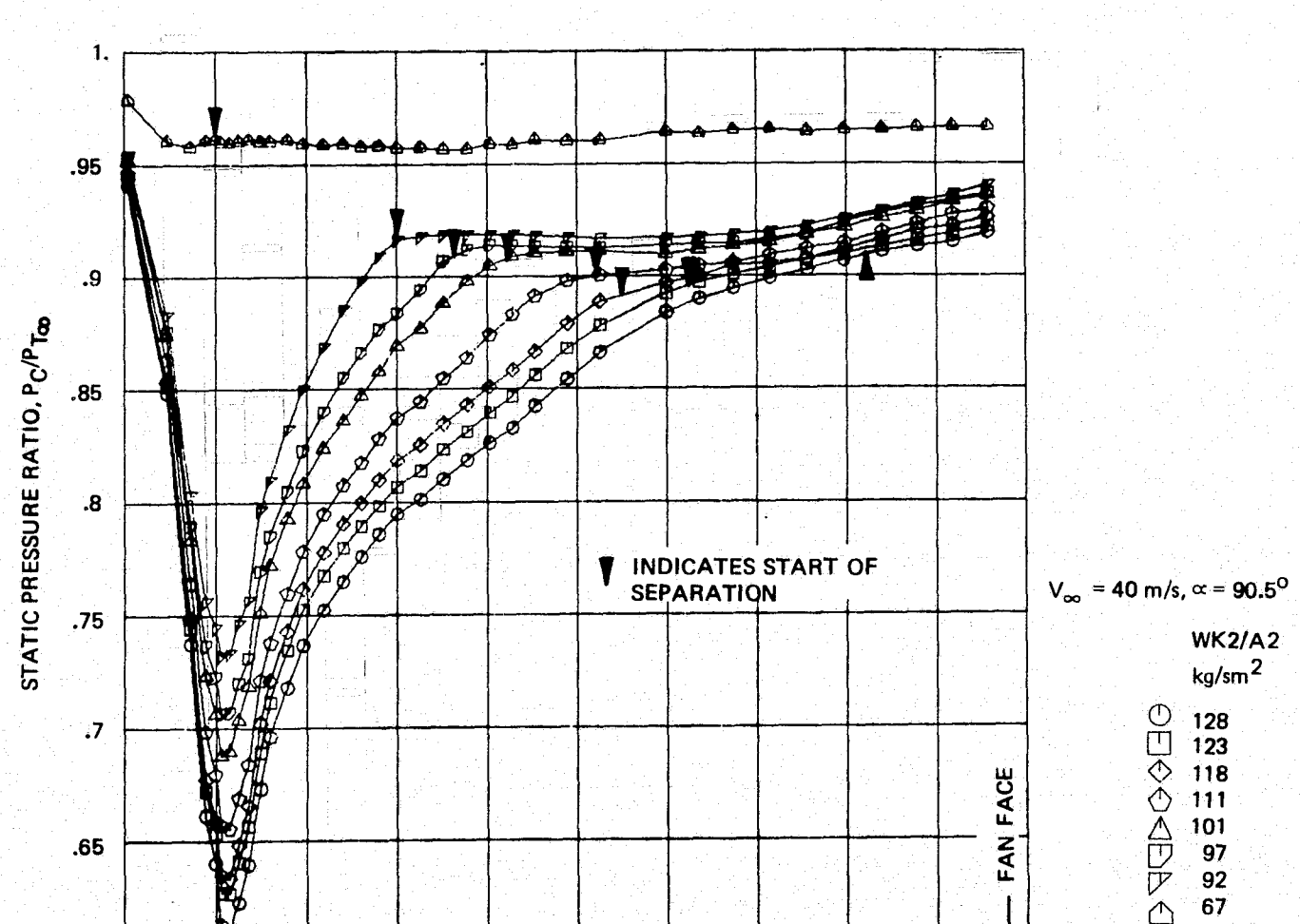

Figure 21. Windward Cowl Static Pressure Profiles With Separated Flow

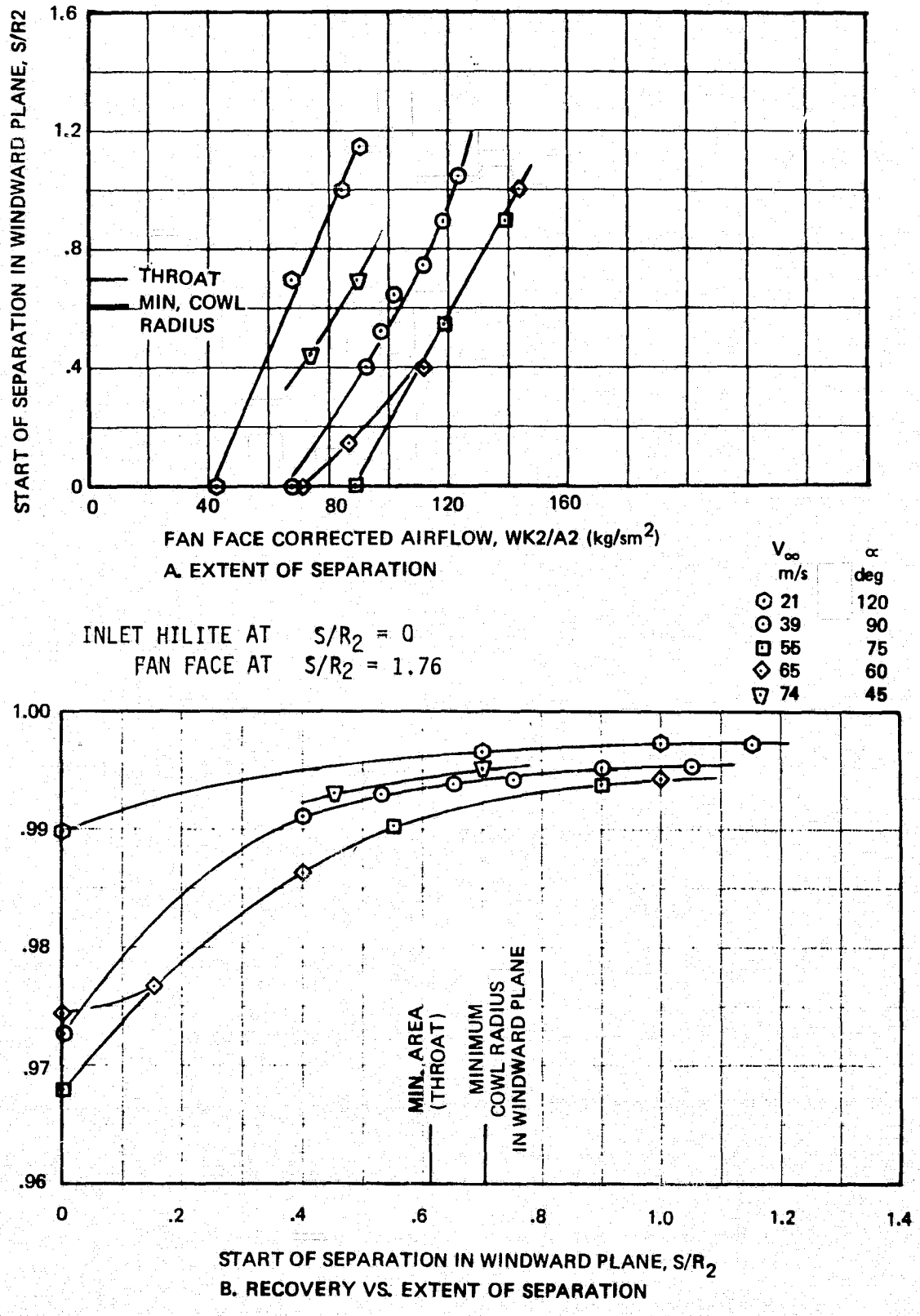

Figure 22. Fan Face Airflow and Recovery Vs. the Extent of Separation

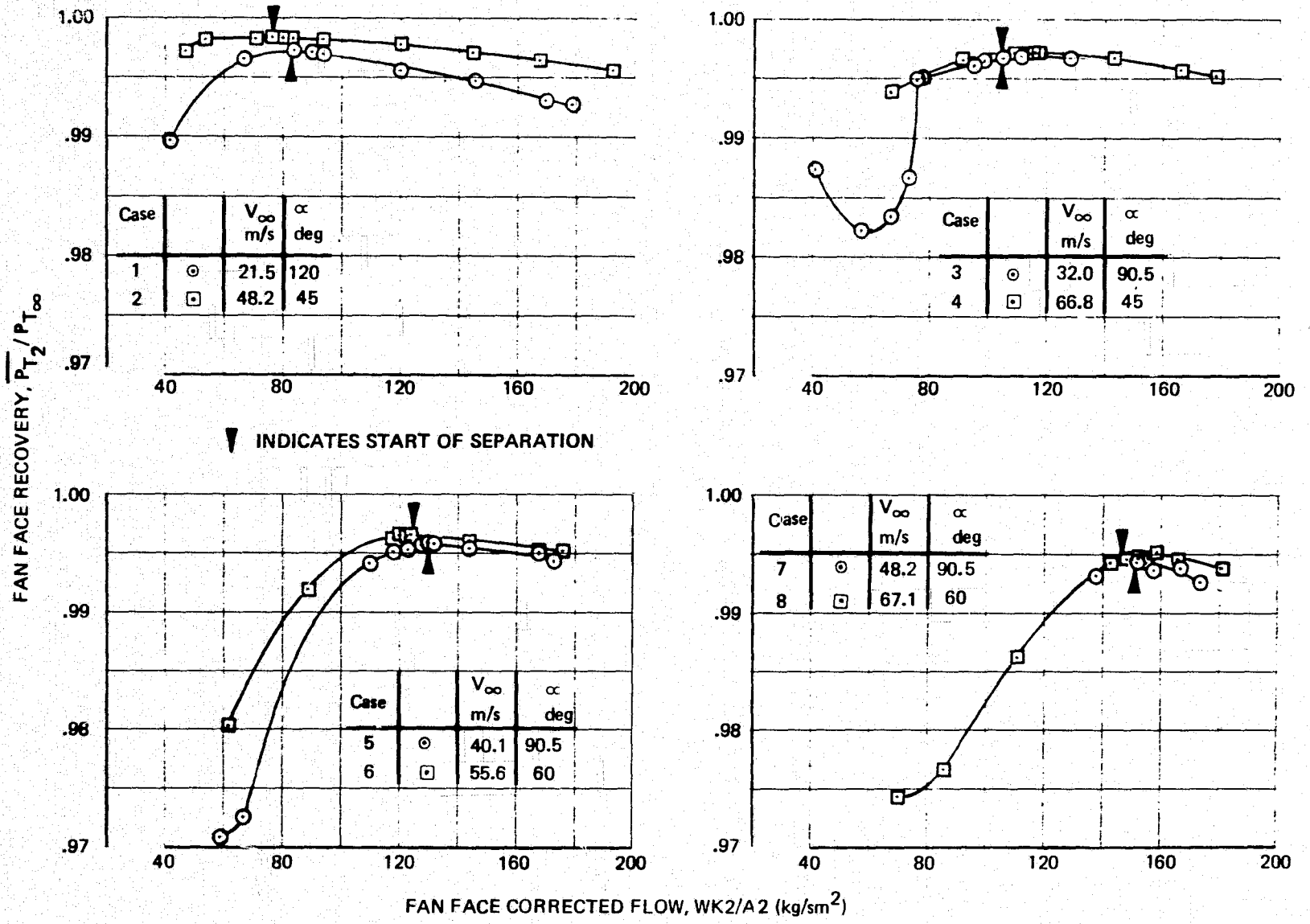

Figure 23. Fan Face Total Pressure Recovery

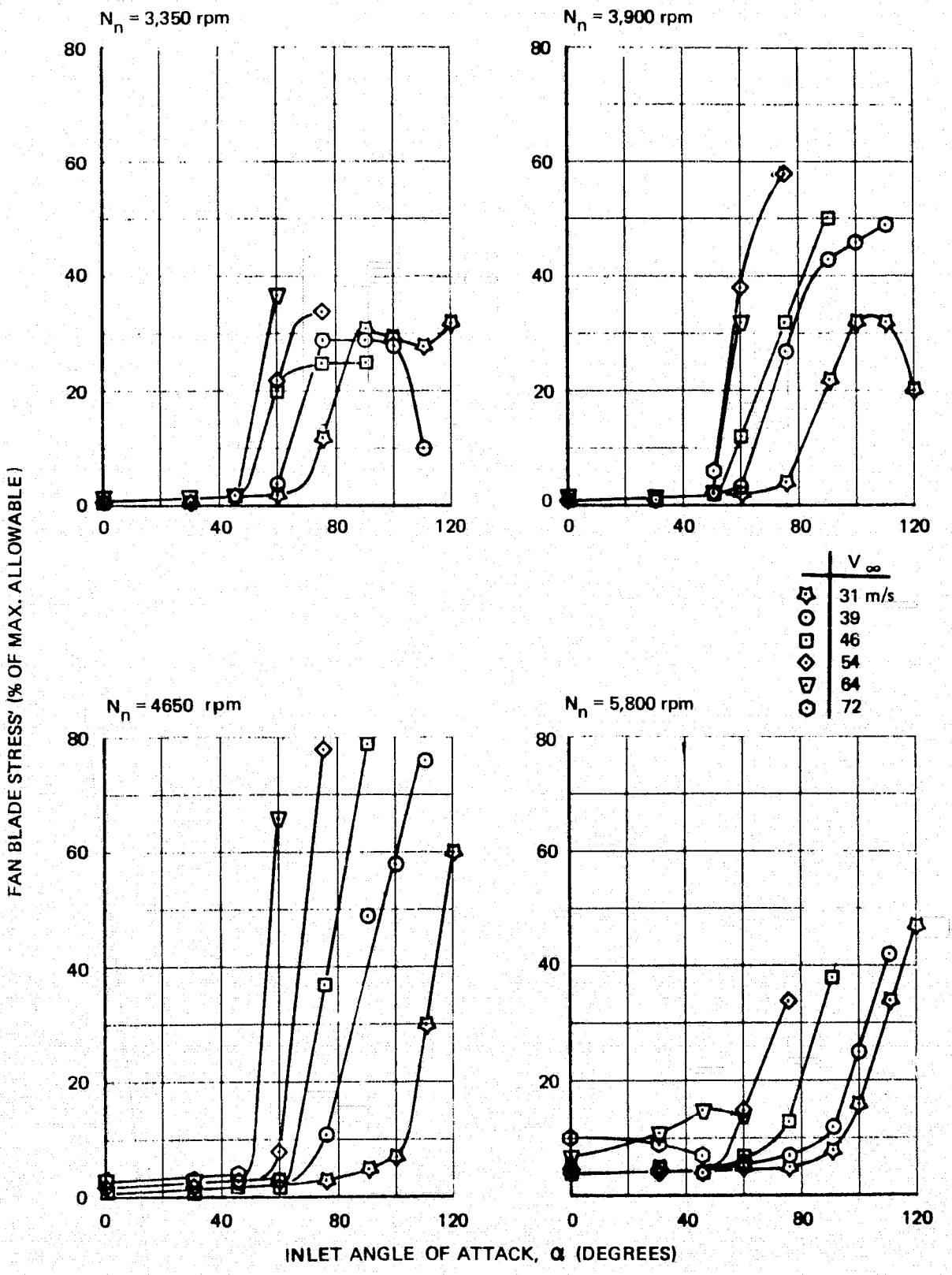

Figure 24. Fan Blade Stresses

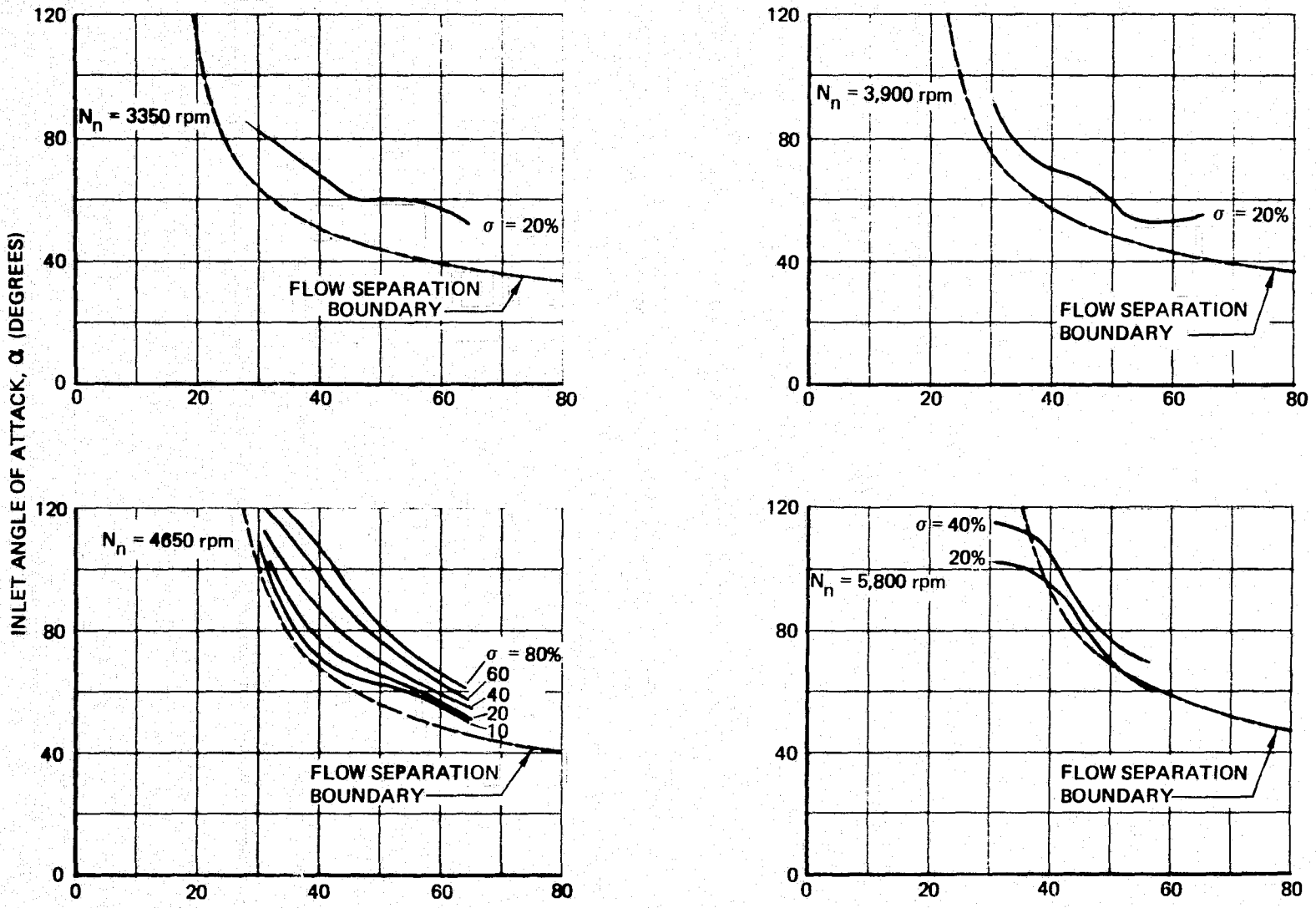

Figure 25. Fan Blade Stress and Flow Separation

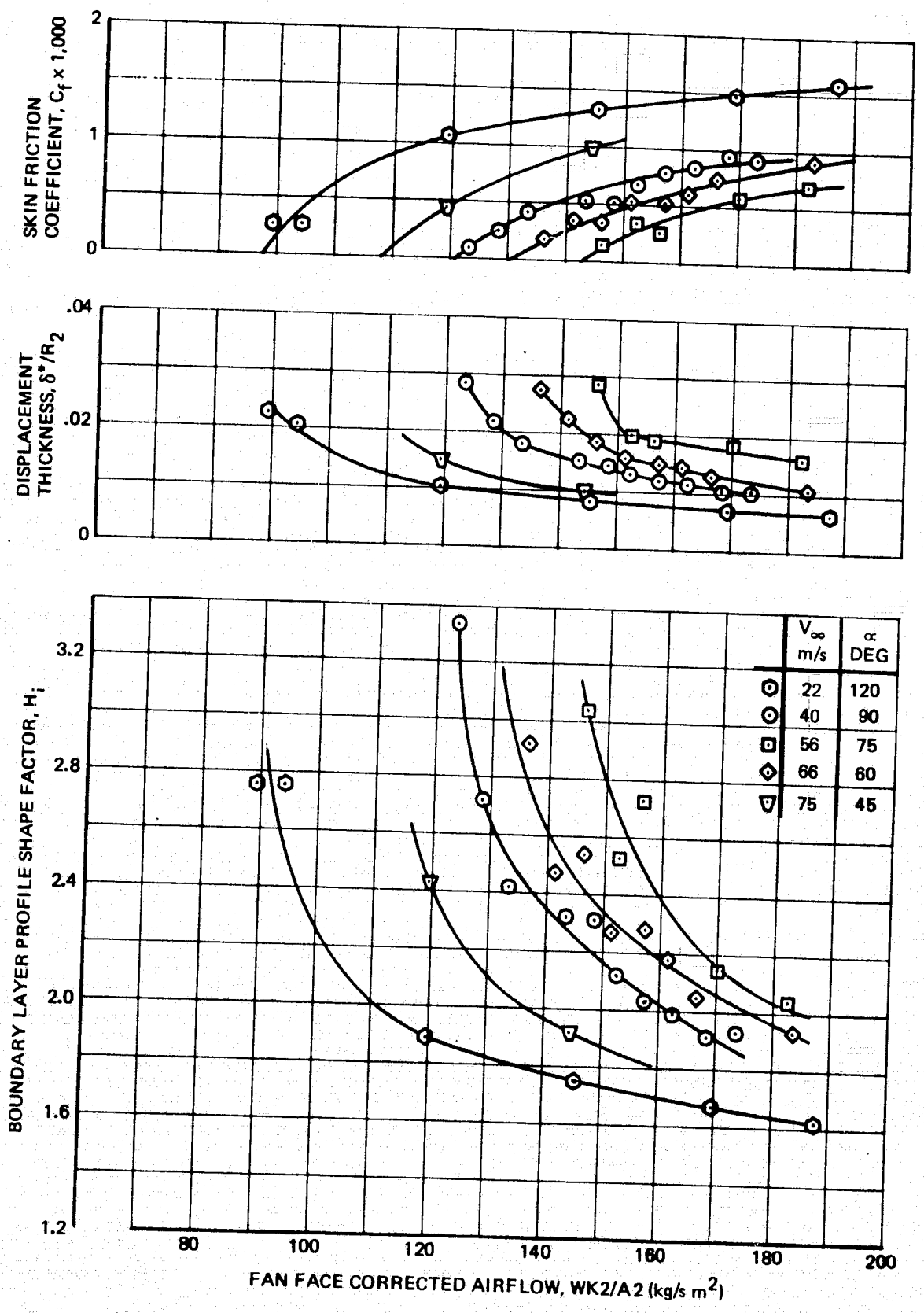

Figure 26. Integral Properties of Measured Boundary Layer Profiles

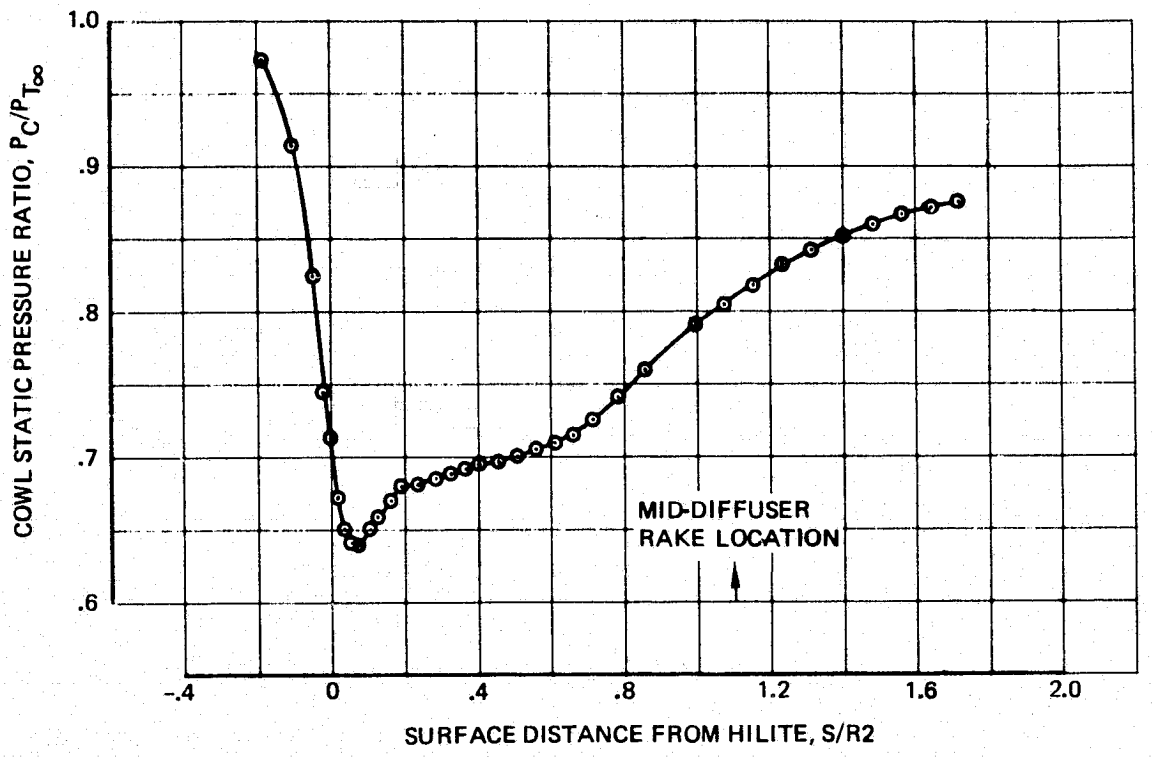

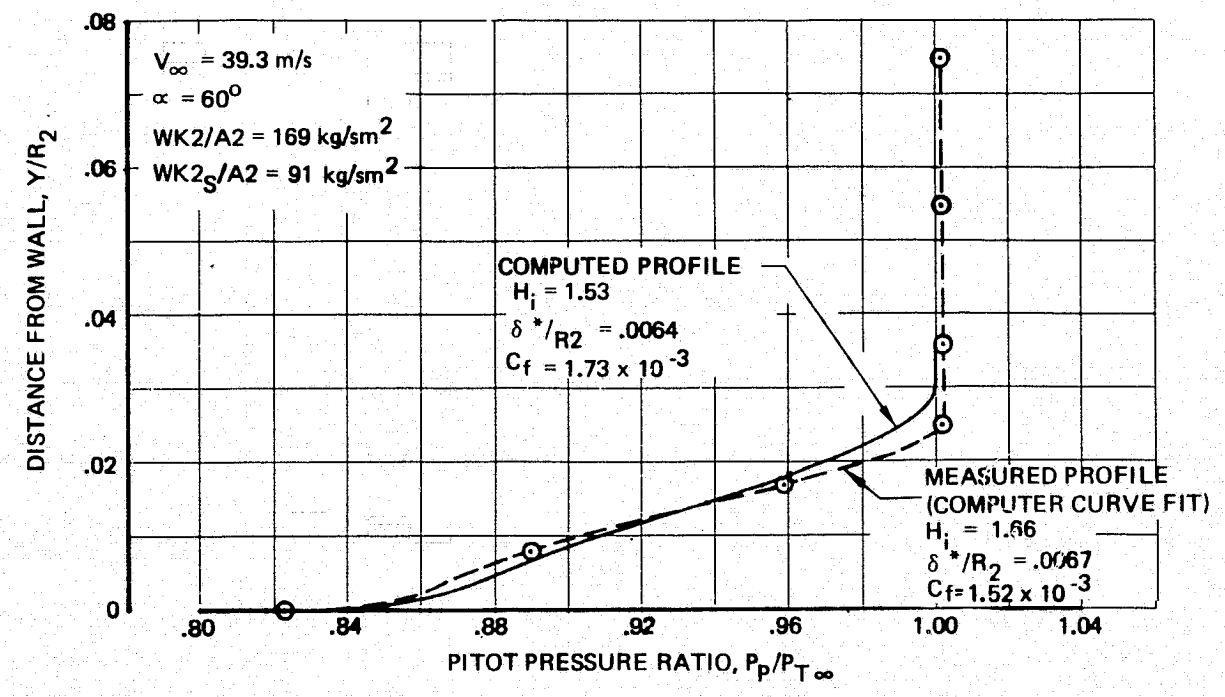

Figure 27. Measured and Computed Profiles, High Airflow

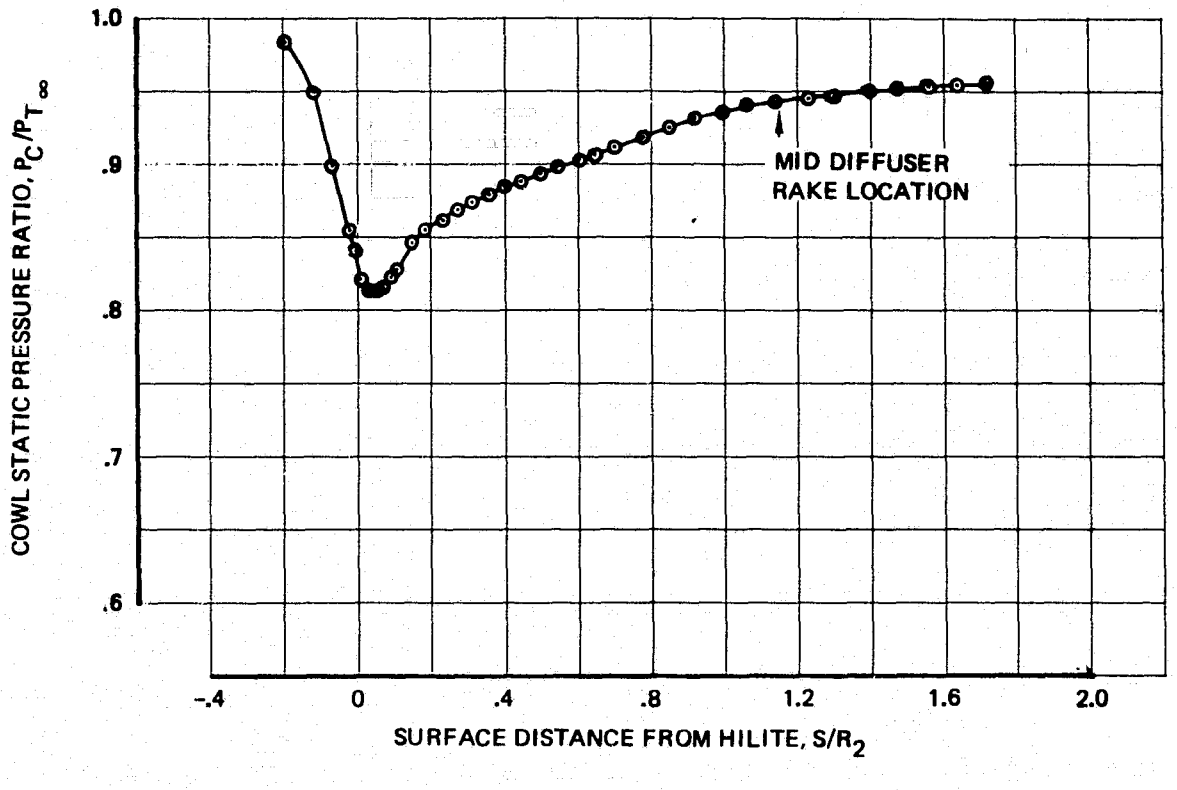

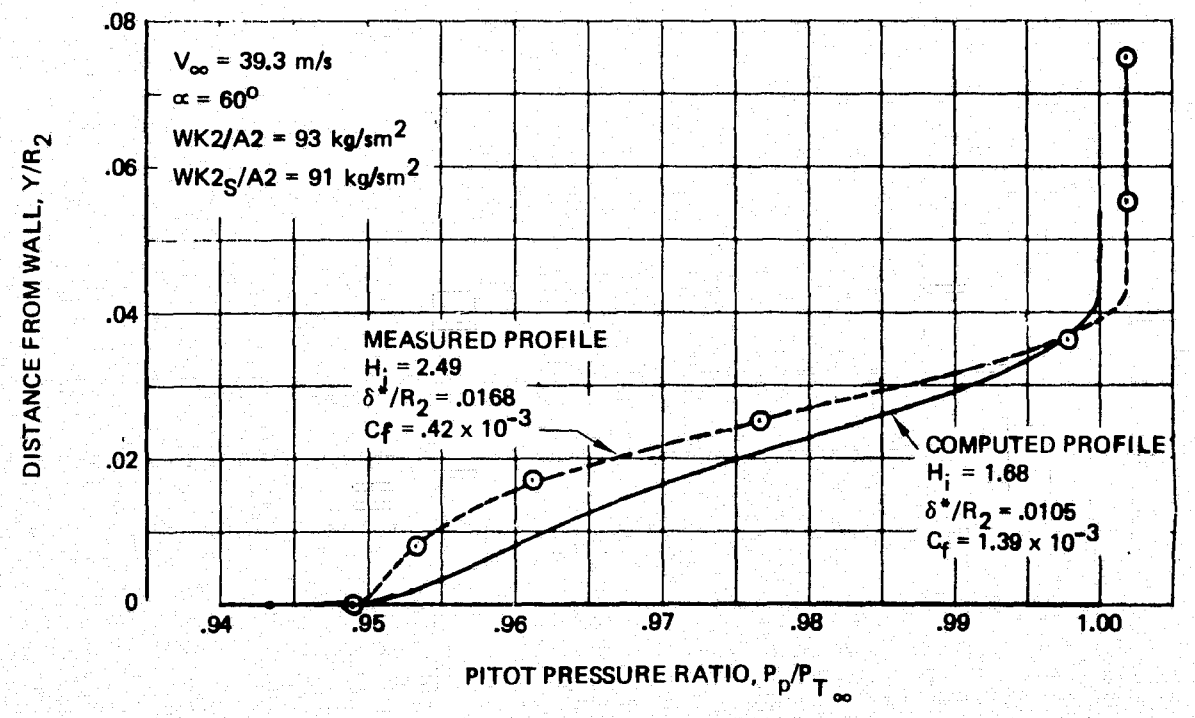

Figure 28. Measured and Computed Profiles, Low Airflow

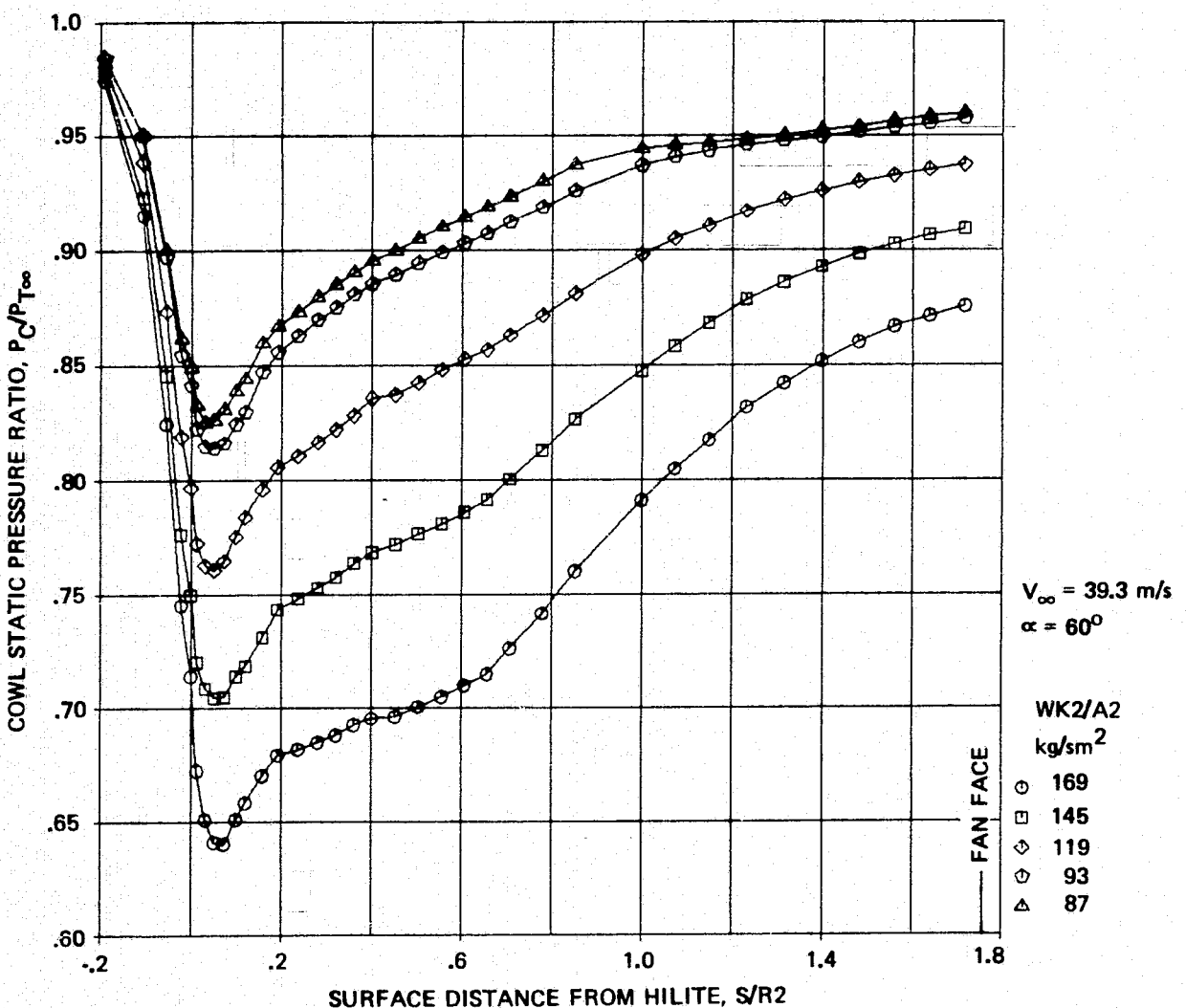

Figure 29. Windward Cowl Static Pressure Profiles

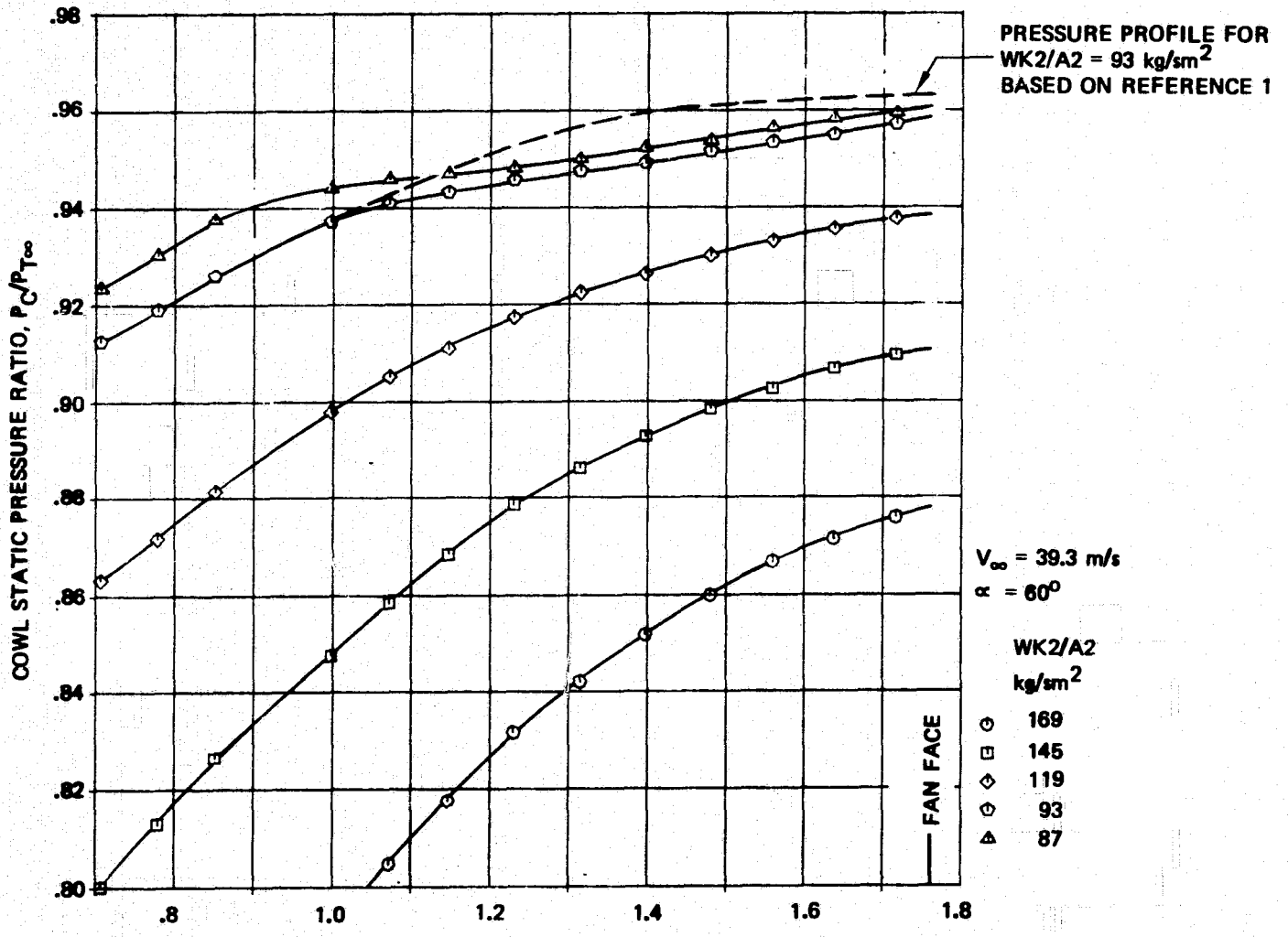

Figure 30. Windward Diffuser Static Pressure Profiles

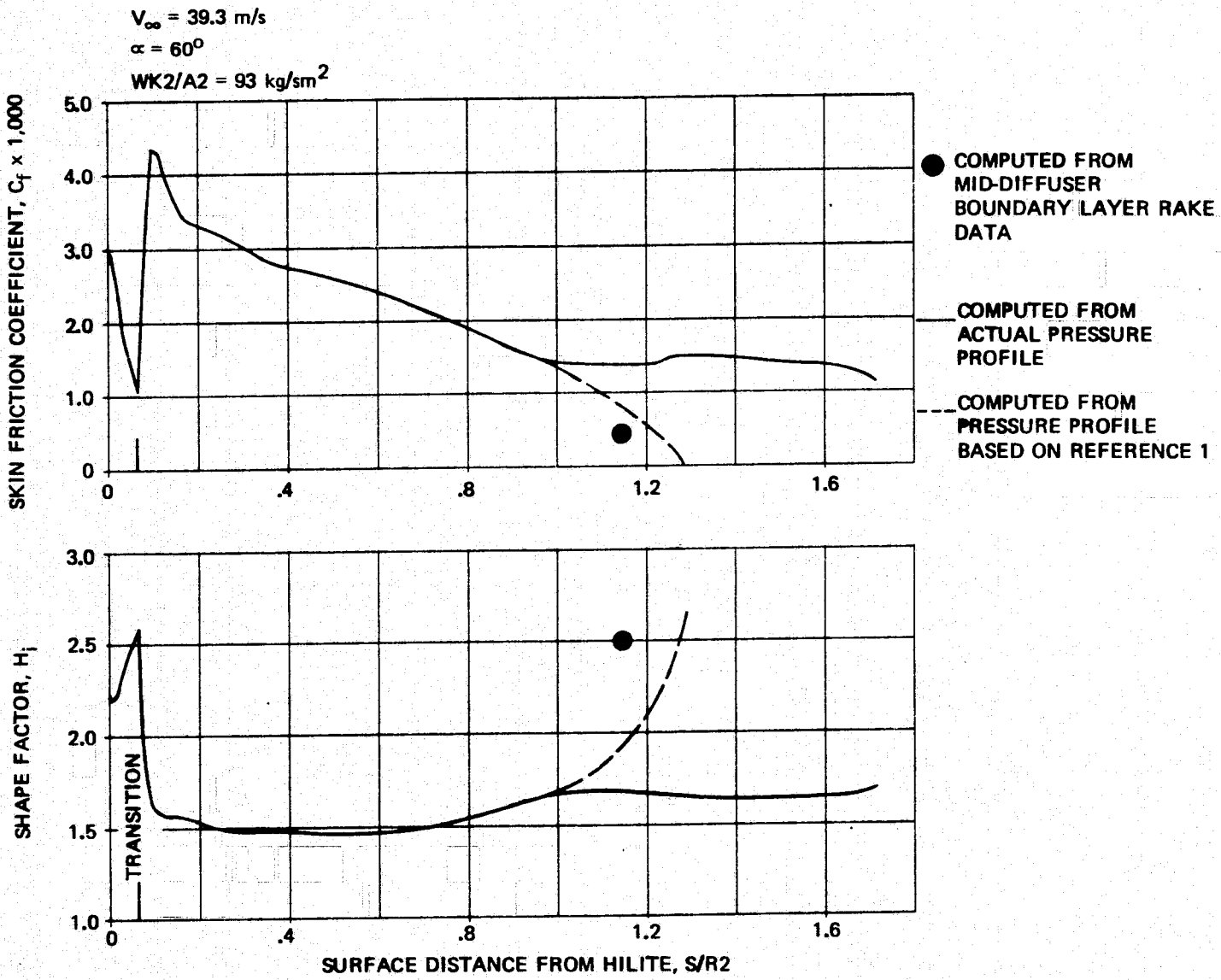

Figure 31. Boundary Layer Development

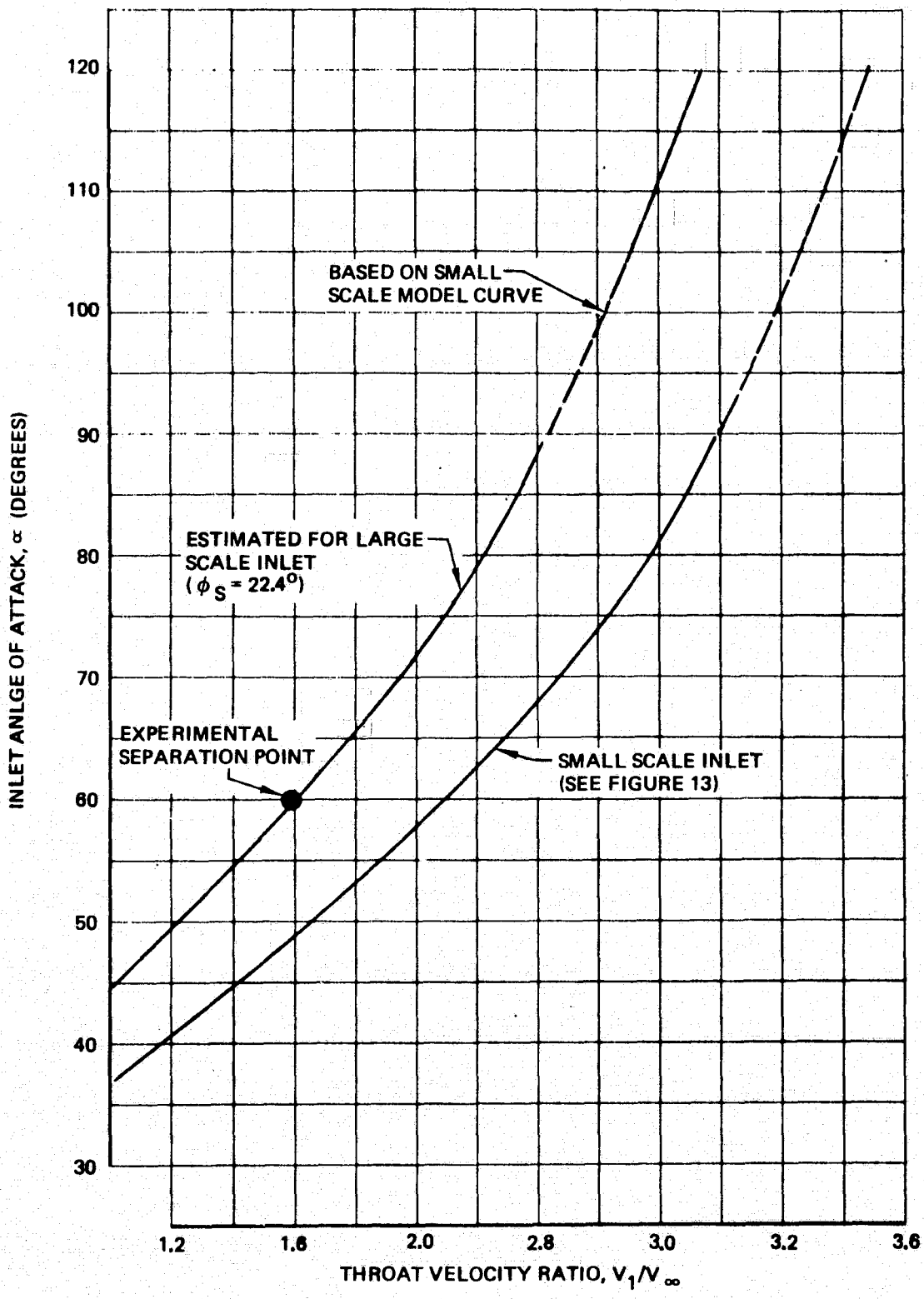

Figure 32. Estimated Separation Boundary for Large Scale Inlet

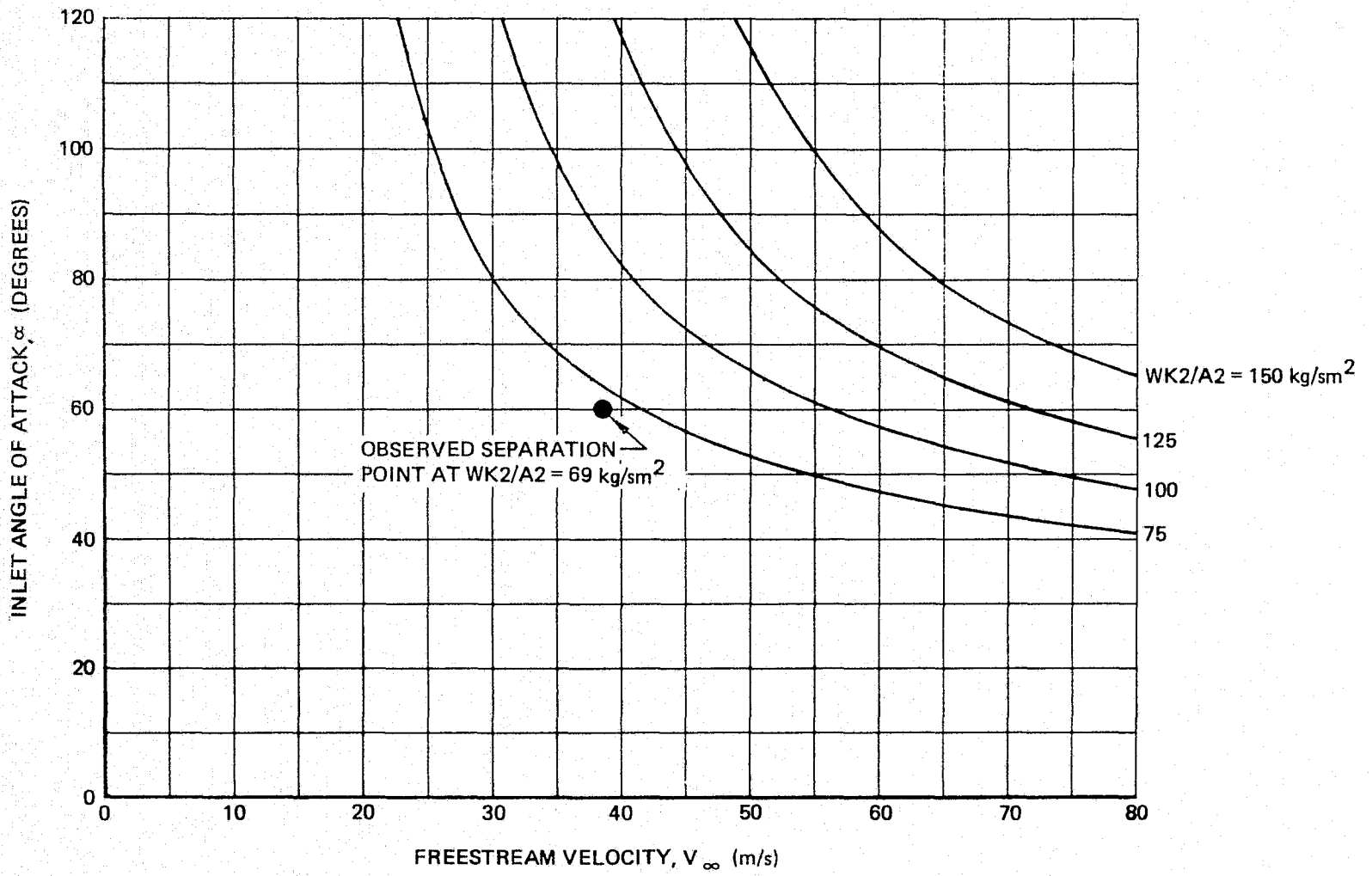

Figure 33. Estimated Separation Boundaries at Constant Airflow for Large Scale Inlet

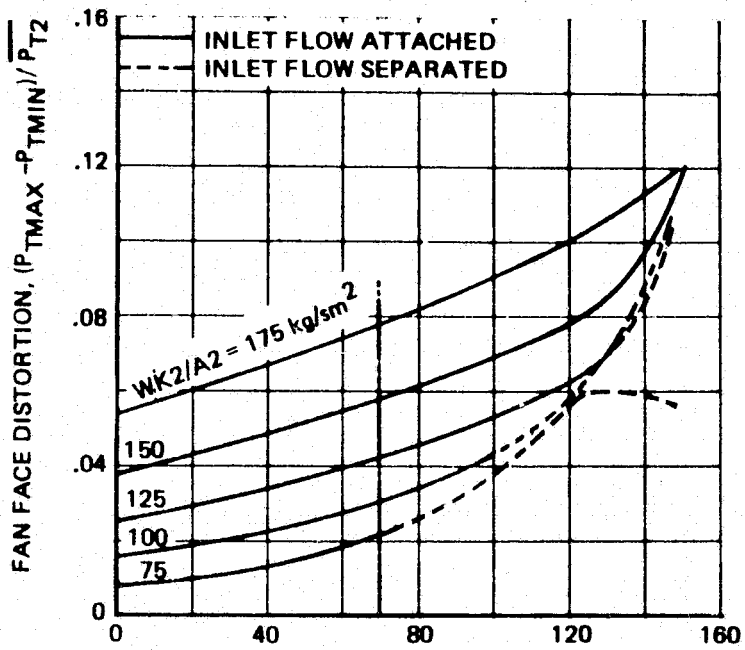

a. DISTORTION SUMMARY

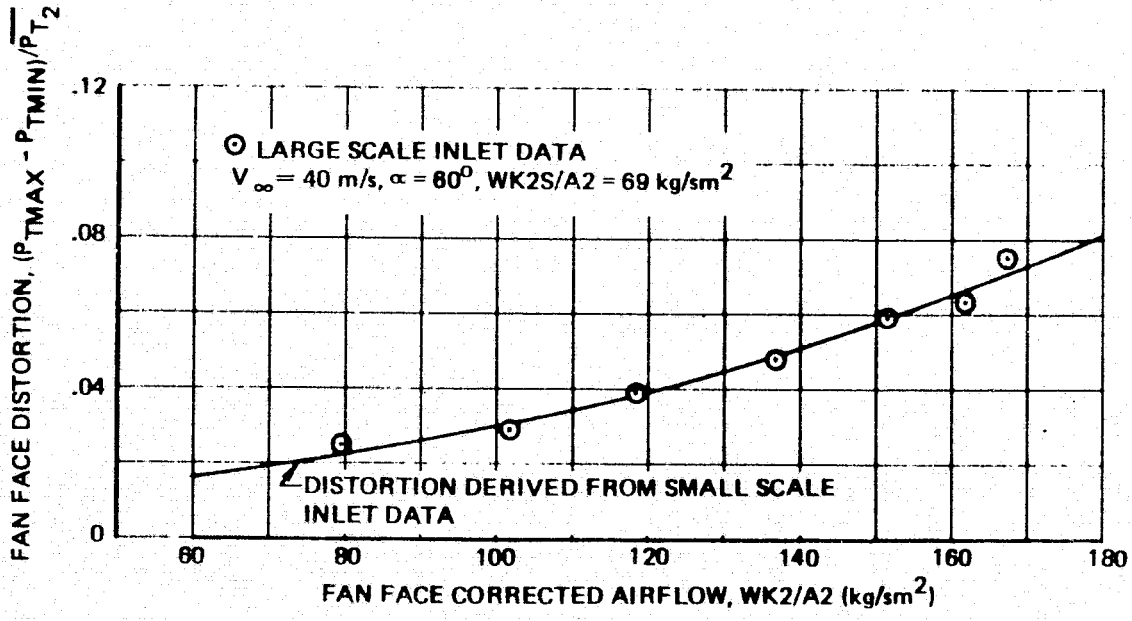

b. COMPARISON OF ESTIMATED DISTORTION WITH DATA

Figure 34. Fan Face Distortion Characteristics